All-vortex nonlinear Compton scattering in a polarized laser field

Yi Liao,[1,2,3,*] Quan-Yu Wang,[1,†] and Yuanbin Wu[1,‡]

[1]*School of Physics, Nankai University, Tianjin 300071, China*

[2]*State Key Laboratory of Nuclear Physics and Technology, Institute of Quantum Matter, South China Normal University, Guangzhou 510006, China*

[3]*Guangdong Basic Research Center of Excellence for Structure and Fundamental Interactions of Matter, Guangdong Provincial Key Laboratory of Nuclear Science, Guangzhou 510006, China*

(Received 12 April 2025; accepted 14 July 2025; published 14 August 2025)

The process of all-vortex nonlinear Compton scattering in an intense and polarized laser field, in which the initial and final electrons and the emitted γ photon are all in vortex states, is studied theoretically. We develop a formalism for the process, which allows us to study the exchanges of the orbital angular momentum (OAM) and spin angular momentum among the electron, γ photon, and laser. A wave packet of the Bessel-Gaussian type is adopted to describe the initial vortex electron for the purpose of normalization. Both circularly and linearly polarized lasers are examined. Substantial numerical calculations are performed to reveal the physics of the exchanges of the OAM and spin angular momentum. The strong impact of the laser intensity and the opening angle of the initial vortex electron is demonstrated. Our results also suggest possible scenarios for the separation of the emitted γ photons with different OAMs, as well as a possible way which could help to distinguish the OAM and spin of the vortex particle by the multipeak structure in the spectrum of the emitted photon.

DOI: 10.1103/gxs8-vgbj

I. INTRODUCTION

A vortex state of a particle or a twisted particle is a quantum state described by the non-plane-wave wave function with a helical phase, and carrying an intrinsic orbital angular momentum (OAM) with respect to the propagation direction [1–8]. Starting from the demonstration of the optical vortex beams in the work of Allen *et al.* in 1992 [9], it has been shown that vortex states of photons [10–21] and massive particles such as electrons [22–27], neutrons [28–30], and atoms [31] can be produced using a number of techniques [3–8], including spiral phase plates, holographic gratings, magnetic monopole fields, and chiral plasmonic near fields. The new degree of freedom represented by the intrinsic OAM of the vortex particles, together with the development of the techniques of the production and manipulation of the vortex states, offers new opportunities for novel effects and opens up numerous applications [3–8], including quantum communications [6–8,32,33] and optical manipulation [6–8,34–36]. This also offers a new and powerful method [3–5,37–55] to study and manipulate the structure of neutrons, protons, and ions, and processes of atomic, nuclear, and particle systems.

So far, the great success of vortex photons and electrons is limited to low energies [5]. This is mainly due to the experimental demonstration and manipulation of vortex photons from visible light to x-ray (on the level of 10 keV) [7–9,13,15–21] and vortex electrons with a kinetic energy up to 300 keV [5,22–24]. Inspired by this and anticipating future experimental progress, high-energy vortex photons and electrons have been envisaged to open up new avenues in high-energy and nuclear physics [5]. High-energy vortex photons and electrons have been shown theoretically to be a novel method to study nuclear and hadronic physics [5,53,55–58], and probe the quantum electrodynamics effects and fundamental aspects of vortex states [5,59–68]. However, the production as well as the detection of high-energy vortex particles so far still remains a challenge [5,69,70], as traditional techniques which work for low energies become impractical at high energies due to problems such as damage thresholds and fabrication complexities. The present proposals for the production of high-energy vortex photons are mainly based on scattering processes, including Compton scattering [71–75], nonlinear Compton scattering in which intense lasers are involved [76–81], and laser-plasma interactions [82–84]. For the production of high-energy vortex electrons, similar methods based on the

*Contact author: liaoy@m.scnu.edu.cn

†Contact author: 1120200055@mail.nankai.edu.cn

‡Contact author: yuanbin@nankai.edu.cn

Published by the American Physical Society under the terms of the Creative Commons Attribution 4.0 International license. Further distribution of this work must maintain attribution to the author(s) and the published article's title, journal citation, and DOI. Funded by SCOAP³.

nonlinear Compton scattering process or laser-plasma interactions have been proposed [69,85], as well as the method of accelerating vortex electrons by the axially symmetric fields of electric and magnetic lenses which could preserve the angular momentum and the shape of a wave packet [86] and the method via generalized measurements or quantum entanglement [87,88].

The process of nonlinear Compton scattering has been considered to be a promising method for the production and investigation of high-energy vortex photons and electrons [69,76–81]. However, full quantum treatments of the process with vortex states have thus far been rather limited [69,78,79]. Here, we study the all-vortex nonlinear Compton scattering in a polarized laser field, in which the initial and final electrons and the emitted γ photon are all in a vortex state. We develop in the Furry picture of quantum electrodynamics a theoretical formalism for the process, which allows us to study the exchanges of the OAM and spin angular momentum among the electron, γ photon, and laser. We adopt a wave packet of the Bessel-Gaussian (BG) type to describe the initial vortex electron for the purpose of normalization, and consider both circularly and linearly polarized lasers. We perform numerical calculations for a relativistic electron, to study the effects of the OAM and spin of the involved particles and the opening angle of the initial vortex electron, as well as the laser intensity. Possible scenarios for the separation of the emitted γ photons with different OAMs are analyzed, as well as the multipeak structure in the emitted photon spectrum which could help to identify the OAM and spin of the vortex particle.

This article is organized as follows. In Sec. II, we present the theoretical formalism for the process of all-vortex nonlinear Compton scattering in which the initial electron is normalized by a BG state. We proceed with differential rates as analytically as we can. Our numerical results are demonstrated in Sec. III by various distributions of the emitted vortex γ photon. Possible scenarios for the separation of emitted γ photons with different OAMs, the features of their spectra, and the exchanges of the OAM and spin angular momentum among the electrons, γ photon, and laser are also discussed. We finally conclude in Sec. IV. The natural units ($\hbar = c = 1$) are used throughout the whole article, and $\alpha = e^2/(4\pi) \sim 1/137$ is the fine-structure constant with e being the electron charge.

II. ANALYTICAL CALCULATION

A. Vortex states and their normalization

We begin with the definitions and conventions for the process under consideration: a vortex electron collides head-on with a monochromatic, plane-wave, strong laser to radiate a vortex photon while continuing to stay in a vortex state. We assume the laser propagates on the $(-z)$ axis with the four-momentum $\Omega^\mu = \omega(1,0,0,-1)$, where ω is its angular frequency. The laser is either linearly polarized, which we choose without loss of generality to be on the x axis,

$$a^\mu(\tau) = M\xi\epsilon_1^\mu \cos\tau, \tag{1}$$

where $\tau = \Omega \cdot x$ and $\epsilon_1^\mu = (0,1,0,0)$ [and $\epsilon_2^\mu = (0,0,1,0)$ for the following use], or circularly polarized which we choose to be left handed,

$$a^\mu(\tau) = \frac{1}{\sqrt{2}} M\xi(\epsilon_1^\mu \cos\tau + \epsilon_2^\mu \sin\tau). \tag{2}$$

Here M is the electron mass, and ξ is a dimensionless parameter so that the electric field strength has the amplitude $E = E_{\rm cr}\xi\omega/M = M\xi\omega/|e|$ with $E_{\rm cr} = M^2/|e|$ being the Schwinger critical field strength. We have chosen for both polarizations the same time average of the electric field squared, $\overline{\mathbf{E}^2} = (M\xi\omega/e)^2/2$, or $|\overline{a^2}| = (M\xi)^2/2$.

1. Bessel-vortex state

In this work we consider first the case in which all of the initial and final electrons and the final photon are in an ideal Bessel-vortex state that is the simplest one that exhibits essential features of a vortex. Since the Bessel vortex is not square integrable, we incorporate a Gaussian smearing to the initial electron vortex, i.e., the so-called Bessel-Gaussian vortex, so that the scattering rate can be well defined. In future work, we will investigate a scenario that would be closer to the experimental situation: the initial electron in a Laguerre-Gauss state collides against a counterpropagating laser pulse that has a finite transverse distance (impact parameter) to the electron.

The kernel of a Bessel vortex is, choosing the z axis as the longitudinal direction [89],

$$a_{\kappa\ell}(\mathbf{p}_\perp) = i^{-\ell} e^{i\ell\phi_p} \sqrt{\frac{2\pi}{\kappa}} \delta(p_\perp - \kappa), \quad p_\perp = |\mathbf{p}_\perp|. \tag{3}$$

Here we denote by a subscript $\perp$ the components of a vector in the transverse xy plane. φ_p is the azimuthal angle in the $\mathbf{p}_\perp$ plane, and κ is a specified magnitude of $\mathbf{p}_\perp$. We take this opportunity to mention an issue of terminology. For a spinless particle, ℓ is an integer that will become in the coordinate representation the projection of intrinsic OAM on the z axis and offers the azimuthal phase characteristic of a vortex state. For a particle with spin, its meaning depends on how we build the part of the wave function associated with the spin degree of freedom which generically also depends on phases involving φ_p. Although it is possible to build a wave function for both the electron and photon in such a way that ℓ in the above kernel corresponds to the projection of the total angular momentum, in this work we follow a different route which fits better our discussion in the background of a laser especially for the emitted vortex photon. In this case a better term for

ℓ would be topological or vortex charge. We mention this because even for a free particle with spin only the projection of total angular momentum can be a conserved quantity. Only in the paraxial limit can both projections of the orbital and spin angular momenta be approximately conserved. Our following analytical analysis does not assume the paraxial approximation, and thus we employ the term topological charge for various ℓ's. Since in our numerical analysis we assume a small opening angle for which the paraxial approximation practically applies, we use interchangeably topological charge and orbital angular momentum.

A Bessel vortex electron that propagates on the z axis has the wave function in free space

$$\psi(x) = e^{i(p_z z - Et)} \int \frac{d^2\mathbf{p}_\perp}{(2\pi)^2} a_{\kappa\ell}(\mathbf{p}_\perp) e^{i\mathbf{p}_\perp\cdot\mathbf{x}_\perp} u(p,\sigma). \quad (4)$$

Here $u(p,\sigma)$ is the usual bispinor that can be built by $u(p,\sigma) = (E+M)^{-1/2}(M+\not{p})u(\mathbf{0},\sigma)$, where $u(\mathbf{0},\sigma)$ (with $\sigma = \pm$) is the normalized bispinor for an electron in its rest frame with spin projection $\sigma/2$ in the z direction. In the Dirac or standard representation [90],

$$u(p,\sigma) = \begin{pmatrix} \sqrt{E+M}\, w_\sigma \\ \sqrt{E-M}\,\hat{\mathbf{p}}\cdot\vec{\sigma} w_\sigma \end{pmatrix}, \quad (5a)$$

$$w_+ = \begin{pmatrix} 1 \\ 0 \end{pmatrix}, \qquad w_- = \begin{pmatrix} 0 \\ 1 \end{pmatrix}, \quad (5b)$$

with $\hat{\mathbf{p}} = \mathbf{p}/|\mathbf{p}|$ and $\sigma^3 w_\sigma = \sigma w_\sigma$. Note that u is normalized by $\bar{u}u = 2M$, and we will handle the normalization of the vortex state soon. Once again we notice that there are two conventional and legitimate choices of the two-component spinor w. Our choice corresponds to that in Refs. [3,91]. We conceive that all plane-wave components of the vortex electron are polarized on the z axis when at rest and are then boosted to form a vortex state. This looks particularly favorable in our following study when a strong laser propagating on the $-z$ axis defines a reference direction. It has been shown in those references that the bispinor adopted here is useful to study the spin-orbit coupling and spin-dependent currents (see also the comment in the Appendix of Ref. [42]), and thus could be more convenient for us to analyze the effects of the spin and orbital angular momenta on our scattering process and their exchanges among the electron, γ photon, and laser. Another choice of w is the one advocated in Ref. [42], which corresponds to helicity eigenstates, and is thus convenient in the study of high-energy scattering.

The presence of a plane-wave laser background specifies a direction in spacetime, and thus not all Descartes components of momentum are conserved between the initial and final states. Following the usual practice, we work with the light-front coordinates to better preserve energy-momentum conservation [92]. As we have assumed the laser propagates on the $(-z)$ axis, we denote for any four-vector $x^\mu = (x^0, \mathbf{x}_\perp, x^3)$,

$$x_\pm = x^0 \pm x^3, \quad (6)$$

where from now on we use the superscripts and subscripts for the $\pm$ components arbitrarily, so that the scalar product, integration measure, and δ functions between the Descartes and light-front coordinates are related by

$$x\cdot y = x^0 y^0 - \mathbf{x}\cdot\mathbf{y} = \frac{1}{2}x_+ y_- + \frac{1}{2}x_- y_+ - \mathbf{x}_\perp\cdot\mathbf{y}_\perp, \quad (7a)$$

$$dx^0 d^3\mathbf{x} = \frac{1}{2} dx_+ dx_- d^2\mathbf{x}_\perp, \quad (7b)$$

$$\delta^4(x-y) = \delta(x^0-y^0)\delta^3(\mathbf{x}-\mathbf{y}) = 2\delta(x_+-y_+)\delta(x_--y_-)\delta^2(\mathbf{x}_\perp-\mathbf{y}_\perp). \quad (7c)$$

In particular the on-shell condition for a particle of momentum p and mass M is, $p^2 = p_+p_- - \mathbf{p}_\perp^2 = M^2$. Employing the light-front coordinates and noting that conservation of the plus component of momentum is not affected by the presence of the laser due to $\Omega_+ = 0$, the Bessel-vortex state for the radiated photon can be designated by k_+ among other quantities:

$$A^\mu_{k_+\kappa_\gamma\ell_\gamma\lambda}(x) = e^{-i(k_+x_- + k_-x_+)/2} \times \int \frac{d^2\mathbf{k}_\perp}{(2\pi)^2} a_{\kappa_\gamma\ell_\gamma}(\mathbf{k}) e^{i\mathbf{k}_\perp\cdot\mathbf{x}_\perp} \Lambda^\mu(k,\lambda). \quad (8)$$

Here $\Lambda^\mu(k,\lambda)$ is the polarization vector for a plane-wave photon of momentum k and helicity λ, which cannot be taken outside of the integral. It is convenient to parametrize it with the help of ϵ_λ and Ω [93,94]:

$$\Lambda(k,\lambda) = \epsilon^*_\lambda - \frac{k\cdot\epsilon^*_\lambda}{k\cdot\Omega}\Omega, \quad (9)$$

where $\epsilon_\lambda = (\epsilon_1 + i\lambda\epsilon_2)/\sqrt{2}$ with $\Lambda(k,\lambda)\cdot k = 0$ and $\Lambda^*(k,\lambda_1)\cdot\Lambda(k,\lambda_2) = -\delta_{\lambda_1\lambda_2}$. κ_γ is the magnitude of its transverse momentum and the integer ℓ_γ denotes its topological charge.

When immersed in a strong plane-wave laser, the so-called Bessel-Volkov solution to the Dirac equation takes into account the laser field exactly. The wave functions for the initial and final electrons are denoted respectively by [49,95]

$$\psi^{(a)}_{p_+\kappa\ell\sigma}(x) = e^{-i(p_+x_- + p_-x_+)/2} \int \frac{d^2\mathbf{p}_\perp}{(2\pi)^2} a_{\kappa\ell}(\mathbf{p}_\perp) e^{i\mathbf{p}_\perp\cdot\mathbf{x}_\perp} e^{i\Phi_p(\tau)} \times \left[1 + \frac{\not{\Omega}\not{a}}{2p\cdot\Omega}\right] u(p,\sigma), \quad (10a)$$

$$\psi^{(a)}_{p'_+\kappa'\ell'\sigma'}(x) = e^{-i(p'_+x_-+p'_-x_+)/2}\int\frac{d^2\mathbf{p}'_\perp}{(2\pi)^2}a_{\kappa'\ell'} \times(\mathbf{p}'_\perp)e^{i\mathbf{p}'_\perp\cdot\mathbf{x}_\perp}e^{i\Phi_{p'}(\tau)}\left[1+\frac{\not{\Omega}\not{a}}{2p'\cdot\Omega}\right]u(p',\sigma'), \tag{10b}$$

where the superscript (a) indicates the presence of the laser background $a^\mu(\tau)$ which introduces an additional phase,

$$\Phi_p(\tau) = \int^\tau d\tau'\left[-\frac{p\cdot a(\tau')}{p\cdot\Omega}+\frac{a^2(\tau')}{2p\cdot\Omega}\right]. \tag{11}$$

Here κ (κ') is the magnitude of the transverse momentum of the initial (final) electron and the integer ℓ (ℓ') denotes its topological charge.

Now we consider normalization and related issues. The normalization of a Bessel-vortex state in free space has been well discussed in the literature [74,89,96]. In the presence of a laser background the normalization of a Bessel-vortex state for a neutral particle is obtained by replacing Descartes components by light-front components; for instance, for the radiated Bessel photon, the normalization factor N^{B}_k to be multiplied to Eq. (8), the number density of states in the interval $dk_\perp dk_+$, and the integration measure in the final-state phase space are respectively

$$N^{\mathrm{B}}_k = \frac{1}{\sqrt{2k_+}}\sqrt{\frac{2\pi}{RL_-}}, \tag{12a}$$

$$dn_k = \frac{Rdk_\perp}{\pi}\frac{L_-dk_+}{4\pi}, \tag{12b}$$

$$(N^{\mathrm{B}}_k)^2dn_k = \frac{dk_\perp dk_+}{2\pi 2k_+}. \tag{12c}$$

Here L_- is a large length of the coordinate component that is conjugate to the conserved plus component of momentum, and R is a large enough radius in the transverse plane beyond which the wave function almost vanishes. Since the vortex state of a charged particle is modified by a strong laser field, we have to recalculate its normalization. For the Bessel-Volkov solution of the electron in Eq. (10a), we calculate the plus component of its current in Appendix A, and it turns out that it yields the same normalization constant as in free space.

2. Bessel-Gaussian vortex state

Finally we discuss the Bessel-Gaussian vortex for the initial electron which is square integrable in the transverse plane, and we employ it for numerical analysis. It is an integral of the wave function in Eq. (10a) over the magnitude κ of the transverse momentum weighted by the Gaussian function $f(\kappa;\kappa_0,\sigma_\perp)$ with the central value κ_0 and deviation $\sigma_\perp$ [97]:

$$\psi^{(a)\mathrm{BG}}_{p_+\kappa_0\sigma_\perp\ell\sigma}(x) = \int_0^\infty d\kappa\,\psi^{(a)}_{p_+\kappa\ell\sigma}(x)f(\kappa;\kappa_0,\sigma_\perp), \tag{13}$$

where

$$f(\kappa;\kappa_0,\sigma_\perp) = N(\kappa_0,\sigma_\perp)\exp\left[-\frac{(\kappa-\kappa_0)^2}{2\sigma_\perp^2}\right], \tag{14}$$

whose square normalization to unity yields

$$N^{-2}(\kappa_0,\sigma_\perp) = \frac{1}{2}\sqrt{\pi}\sigma_\perp\left[1+\mathrm{erf}\left(\frac{\kappa_0}{\sigma_\perp}\right)\right]. \tag{15}$$

Since we require that the Bessel-Gaussian vortex be on shell and p_+ be a good quantum number in the presence of a laser, smearing in κ implies variation in p_- according to $p_+p_- - \kappa^2 = M^2$.

The issue of normalization has to be reconsidered for a Bessel-Volkov solution whose magnitude of transverse momentum is Gaussian smeared, i.e., Eq. (13), where the Bessel-Volkov solution $\psi^{(a)}_{p_+\kappa\ell\sigma}$ is expressed in Eq. (A1) (without the normalization factor N^{B}_p of course). When forming the plus component of the current, $j_+ = \bar\psi^{(a)\mathrm{BG}}_{p_+\kappa_0\sigma_\perp\ell\sigma}\gamma_+\psi^{(a)\mathrm{BG}}_{p_+\kappa_0\sigma_\perp\ell\sigma}$, we notice several points that are different from the pure Bessel-Volkov case. We denote by a tilde all momentum-dependent quantities in $\bar\psi^{(a\mathrm{BG})}_{p_+\kappa_0\sigma_\perp\ell\sigma}$; for instance, the Gaussian integration variable in $\bar\psi^{(a\mathrm{BG})}_{p_+\kappa_0\sigma_\perp\ell\sigma}$ is $\tilde\kappa$. With a fixed p_+, $p\cdot\Omega = p_+\Omega_-/2$ is also fixed. This results in simplifications in j_+. For instance, the phase ϕ^p_a stays intact from smearing and the variable $\mathcal{R}_\perp$ is the same in both $\bar\psi^{(a)\mathrm{BG}}_{p_+\kappa_0\sigma_\perp\ell\sigma}$ and $\psi^{(a)\mathrm{BG}}_{p_+\kappa_0\sigma_\perp\ell\sigma}$; for relevant definitions, see Appendix A. We obtain

$$j_+(x) = \int d\kappa\int d\tilde\kappa f\tilde f e^{i(\tilde p_- - p_-)x_+/2}\sqrt{\frac{\kappa\tilde\kappa}{(2\pi)^2}} \times[(\tilde\epsilon_+ + \tilde\epsilon_-\tilde c)(\epsilon_+ + \epsilon_- c)J_\ell(\kappa\mathcal{R}_\perp)J_\ell(\tilde\kappa\mathcal{R}_\perp) + \tilde\epsilon_-\epsilon_-\tilde s s J_{\ell+\sigma}(\kappa\mathcal{R}_\perp)J_{\ell+\sigma}(\tilde\kappa\mathcal{R}_\perp)], \tag{16}$$

where $c = \cos\theta_p$, $\tilde s = \sin\theta_{\tilde p}$, etc. Using [98]

$$\int_0^\infty xdx\,J_\ell(\kappa x)J_\ell(\kappa' x) = \frac{1}{\kappa}\delta(\kappa-\kappa'), \tag{17}$$

and transforming integration over $\mathbf{x}_\perp$ to that over $\boldsymbol{\mathcal{R}}_\perp$ as in Appendix A, all complications arising from smearing disappear:

$$\int \frac{1}{2} dx^- d^2\mathbf{x}_\perp j_+(x) = \frac{L_-}{2} \int 2\pi \mathcal{R}_\perp d\mathcal{R}_\perp j_+(x) = \frac{L_-}{2} 2p^+. \tag{18}$$

This is as nice as anticipated: the state is normalized in the transverse plane of space and is normalized as for a plane wave on the minus axis. In summary, for the Bessel photon and Bessel-Volkov electron states we employ the normalization factor as in Eq. (12a) and for the initial Bessel-Volkov electron whose magnitude of transverse momentum is smeared we employ the normalization factor

$$N_p^{\mathrm{BG}} = \frac{1}{\sqrt{2p_+}} \sqrt{\frac{2}{L_-}}. \tag{19}$$

B. Scattering amplitude for plane-wave electrons and photon

Since a vortex state is a linear composition of infinitely many plane-wave states, the S matrix element for a process involving vortex states, S_{B}, can be constructed from that involving only plane-wave states, S_{pw}. For the simplest case of pure Bessel-vortex states and without taking into account differences in normalization for the moment, we have for the process under consideration [89]

$$S_{\mathrm{B}} = \int \frac{d^2\mathbf{p}_\perp}{(2\pi)^2} \int \frac{d^2\mathbf{p}'_\perp}{(2\pi)^2} \int \frac{d^2\mathbf{k}_\perp}{(2\pi)^2} a^\dagger_{\kappa_\gamma \ell_\gamma} \times (\mathbf{k}_\perp) a^\dagger_{\kappa'\ell'}(\mathbf{p}'_\perp) a_{\kappa\ell}(\mathbf{p}_\perp) S_{\mathrm{pw}}, \tag{20}$$

where

$$S_{\mathrm{pw}} = -ie \int d^4x\, e^{-iP\cdot x} e^{i[\Phi_p(\tau) - \Phi_{p'}(\tau)]} U, \tag{21a}$$

$$U = \Lambda^\mu(k,\lambda) \overline{u(p',\sigma')} \left[1 + \frac{\not{a}\not{\Omega}}{2p'\cdot\Omega}\right] \gamma_\mu \left[1 + \frac{\not{\Omega}\not{a}}{2p\cdot\Omega}\right] u(p,\sigma), \tag{21b}$$

and $P = p - p' - k$. In the following we first compute the bilinear form U, and then treat the phases and finish integration over the coordinate x.

1. Bilinear

Since the laser quadratic term $O(a^2)$ in Eq. (21b) does not survive using $\not{\Omega}\not{\epsilon}^*_\lambda\not{\Omega} = 0$ and $\not{\Omega}\not{\Omega} = 0$, the bilinear becomes,

$$U = [2(E+M)(E'+M)]^{-1/2}(B_0 + \sqrt{2}\mathbf{a}_\perp \cdot \vec{\epsilon}^*_\lambda B_1), \tag{22}$$

where for the electron spin-preserved case ($\sigma' = \sigma$),

$$B_0 = -2\delta_{\lambda\bar{\sigma}}(E'+M)p_\sigma - 2\delta_{\lambda\sigma}(E+M)p'_{\bar{\sigma}} + r_\lambda[(p'_+ + M)(p_+ + M) + (\mathbf{p}'_\perp \cdot \mathbf{p}_\perp + i\sigma R^3)], \tag{23a}$$

$$B_1 = +\left(\frac{\delta_{\lambda\sigma}}{p'_+} + \frac{\delta_{\lambda\bar{\sigma}}}{p_+}\right)(p'_+ + M)(p_+ + M) + \left(\frac{\delta_{\lambda\bar{\sigma}}}{p'_+} + \frac{\delta_{\lambda\sigma}}{p_+}\right)(\mathbf{p}'_\perp \cdot \mathbf{p}_\perp + i\sigma R^3), \tag{23b}$$

and for the electron spin-flipped case ($\sigma' = -\sigma$),

$$B_0 = 2\sigma\delta_{\lambda\sigma}[(p_+ + M)p'^3 - (p'_+ + M)p^3] + r_\lambda\sigma[(p_+ + M)p'_\sigma - (p'_+ + M)p_\sigma], \tag{24a}$$

$$B_1 = -\sigma\left(\frac{\delta_{\lambda\bar{\sigma}}}{p'_+} + \frac{\delta_{\lambda\sigma}}{p_+}\right)(p'_+ + M)p_\sigma + \sigma\left(\frac{\delta_{\lambda\sigma}}{p'_+} + \frac{\delta_{\lambda\bar{\sigma}}}{p_+}\right)(p_+ + M)p'_\sigma. \tag{24b}$$

Both B_0 and B_1 are independent of the laser parameters which enter only in the global factor $\sqrt{2}\mathbf{a}_\perp \cdot \vec{\epsilon}^*_\lambda$. Note that the laser polarization is determined by $\mathbf{a}_\perp$ while ϵ^μ_λ is an auxiliary vector that depends on the helicity λ of the radiated photon. We have introduced the following abbreviations:

$$\bar{\lambda} = -\lambda, \quad \bar{\sigma} = -\sigma, \quad r_\lambda = \frac{1}{k_+}\mathbf{k}_\perp \cdot \sqrt{2}\vec{\epsilon}^*_\lambda, \tag{25a}$$

$$\mathbf{R} = \mathbf{p}' \times \mathbf{p}, \quad R_\sigma = R^1 + i\sigma R^2, \tag{25b}$$

$$p_\sigma = p^1 + i\sigma p^2, \quad p'_\sigma = p'^1 + i\sigma p'^2. \tag{25c}$$

2. Phases

There are two types of phases in Eq. (21a): one is from the usual plane-wave

$$-P\cdot x = -\frac{1}{2}P_+ x_- - \frac{1}{2}P_- x_+ + \mathbf{P}_\perp \cdot \mathbf{x}_\perp, \tag{26}$$

and the other is introduced by the Volkov solution, which becomes after some algebra

$$\Phi^{(a)} = \Phi_p(\tau) - \Phi_{p'}(\tau) = \int^\tau d\tau' \left[-\frac{k\cdot a}{p'\cdot\Omega} + \frac{k\cdot\Omega}{p'\cdot\Omega p\cdot\Omega}\left(p\cdot a - \frac{1}{2}a^2\right)\right]. \tag{27}$$

The laser introduces nontrivial x dependence through $\tau = \Omega\cdot x = \Omega^- x^+/2 = \omega(x^0 + x^3)$. Thus the x components other than x^+ can be finished to the δ functions as

usual; in other words, the minus components of the particles' momenta are not conserved due to their exchange with the laser while the other three components are still conserved. To incorporate all components in a uniform manner, we follow Ref. [93] to introduce a parameter integral:

$$\int \Omega^- du\, \delta(u\Omega^- + P^-) = 1. \tag{28}$$

Since all components of Ω other than Ω^- vanish, the above δ function can be combined with the other three from integration over x^- and $\mathbf{x}_\perp$ into

$$\delta^4(u\Omega + P) = 2\delta(u\Omega^- + P^-)\delta(P^+)\delta^2(\mathbf{P}_\perp), \tag{29}$$

which yields three equivalent answers for u:

$$u = -\frac{P^-}{\Omega^-} = \frac{k\cdot p}{p'\cdot\Omega} = \frac{k\cdot p'}{p\cdot\Omega}. \tag{30}$$

To summarize what we have achieved so far,

$$S_{\rm pw} = -ie\int\frac{du}{2\pi}\int d\tau(2\pi)^4\delta^4(u\Omega+P)e^{i[u\tau+\Phi^{(a)}]}U. \tag{31}$$

To proceed further, we have to work out the laser-dependent phase $\Phi^{(a)}$. For the circularly polarized laser in Eq. (2), we have

$$\Phi^{(a)} = 2\beta\tau - \gamma^{\rm C}\sin(\tau-\tau_\rho), \tag{32}$$

where the following notations are introduced:

$$\beta = \frac{k_+(M\xi)^2}{8p_+p'_+\omega}, \qquad \gamma^{\rm C} = \frac{p_+M\xi}{\sqrt{2}p'_+\omega}\rho, \tag{33a}$$

$$\vec{\rho} = \frac{k_+}{p_+}\frac{\mathbf{p}_\perp}{p_+} - \frac{\mathbf{k}_\perp}{p_+} = \rho(\cos\tau_\rho, \sin\tau_\rho). \tag{33b}$$

For the linearly polarized laser in Eq. (1), we obtain

$$\Phi^{(a)} = 2\beta\tau - \gamma^{\rm L}\sin\tau + \beta\sin(2\tau), \tag{34}$$

where

$$\gamma^{\rm L} = \frac{M\xi}{p'\cdot\Omega}\left[k\cdot\epsilon_1 - \frac{k\cdot\Omega}{p\cdot\Omega}p\cdot\epsilon_1\right] = \sqrt{2}\gamma^{\rm C}\cos\tau_\rho. \tag{35}$$

3. Plane-wave amplitude

To facilitate the τ integral, we notice that the triangular terms in $\Phi^{(a)}$ are periodic functions of τ, so that their phase factors in $\exp[i\Phi^{(a)}]$ should be expanded in integer powers of $e^{i\tau}$. By using [99]

$$e^{iz\sin\theta} = \sum_{n=-\infty}^{\infty} J_n(z)e^{in\theta}, \tag{36}$$

we have for the circularly polarized laser,

$$e^{-i\gamma^{\rm C}\sin(\tau-\tau_\rho)} = \sum_{n=-\infty}^{\infty} J_n(\gamma^{\rm C})e^{-in\tau}e^{in\tau_\rho}, \tag{37a}$$

$$e^{\pm i\tau}e^{-i\gamma^{\rm C}\sin(\tau-\tau_\rho)} = \sum_{n=-\infty}^{\infty} J_{n\pm1}(\gamma^{\rm C})e^{-in\tau}e^{i(n\pm1)\tau_\rho}, \tag{37b}$$

and for the linearly polarized laser,

$$e^{i[-\gamma^{\rm L}\sin\tau+\beta\sin(2\tau)]} = \sum_{n,\nu=-\infty}^{\infty} e^{-in\tau}J_{2\nu+n}(\gamma^{\rm L})J_\nu(\beta), \tag{38a}$$

$$e^{i[-\gamma^{\rm L}\sin\tau+\beta\sin(2\tau)]}\cos\tau = \frac{1}{2}\sum_{n,\nu=-\infty}^{\infty} e^{-in\tau}[J_{2\nu+n-1}(\gamma^{\rm L}) + J_{2\nu+n+1}(\gamma^{\rm L})]J_\nu(\beta), \tag{38b}$$

where the $e^{\pm i\tau}$ or $\cos\tau$ factor is anticipated in the linear a term of the bilinear U.

The τ integral can now be finished to yield $\delta(u+2\beta-n)$ for both polarizations of the laser, which in turn is used to finish the u integral in terms of $u_n = n-2\beta$. Since $u+2\beta>0$, the summation over n is actually restricted to $n\geq n_0$ where n_0 is some positive integer. The scattering matrix in the plane-wave case becomes finally,

$$S^{\rm P}_{\rm pw} = -ie\frac{(2\pi)^4 2\delta(P^+)\delta^2(\mathbf{P}_\perp)}{\sqrt{2(E+M)(E'+M)}} \times\sum_{n=n_0}^{+\infty}\delta(u_n\Omega^- + P^-)(\mathcal{A}^{\rm P}_{0n} + |a|\mathcal{A}^{\rm P}_{1n}), \tag{39}$$

where the superscript P refers to the case of a linearly polarized laser P = L,

$$\mathcal{A}^{\rm L}_{0n} = B_0\sum_{\nu=-\infty}^{\infty} J_\nu(\beta)J_{2\nu+n}(\gamma^{\rm L}), \tag{40a}$$

$$\mathcal{A}^{\rm L}_{1n} = \frac{1}{2}B_1\sum_{\nu=-\infty}^{\infty} J_\nu(\beta)(J_{2\nu+n-1}(\gamma^{\rm L}) + J_{2\nu+n+1}(\gamma^{\rm L})), \tag{40b}$$

or the case of a circularly polarized laser P = C,

$$\mathcal{A}^{\rm C}_{0n} = B_0 J_n(\gamma^{\rm C})e^{in\tau_\rho}, \tag{41a}$$

$$\mathcal{A}^{\rm C}_{1n} = \frac{1}{\sqrt{2}}B_1 J_{n-\lambda}(\gamma^{\rm C})e^{i(n-\lambda)\tau_\rho}. \tag{41b}$$

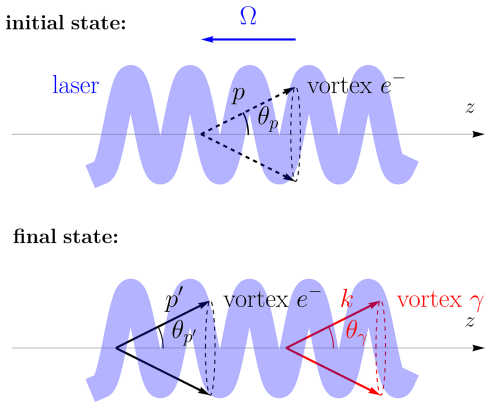


FIG. 1. A vortex electron of opening angle θ_p collides head-on against a strong plane-wave laser to become a vortex electron of opening angle $\theta_{p'}$ while radiating a vortex photon of opening angle θ_k.

C. Scattering amplitude for Bessel-vortex electrons and photon

We are now in a position to calculate analytically the all-vortex nonlinear Compton scattering in a strong and polarized laser. The laser is approximated by a monochromatic plane wave propagating in the $-z$ direction whose effect on the electron has been completely taken into account without expansion in the number of laser photons. We assume that the initial and final vortex electrons and the emitted vortex photon propagate in the z direction and share the same vortex line. This is a technical simplification. In future work we will consider the general case when the final vortex particles have a finite scattering angle and a vortex line deviating from the initial beam direction. For clarity we show the scattering geometry in Fig. 1.

By using Eqs. (20) and (39), the S matrix in the Bessel-vortex case becomes

$$S_{\mathrm{B}}^{\mathrm{P}} = -ie\sum_{n=n_0}^{\infty}\int\frac{d^2\mathbf{p}_\perp}{(2\pi)^2}\int\frac{d^2\mathbf{p}'_\perp}{(2\pi)^2} \times\int\frac{d^2\mathbf{k}_\perp}{(2\pi)^2}(2\pi)^4\delta^4(u_n\Omega+P)F^{\mathrm{P}}(\varphi,\varphi',\varphi_k), \tag{42}$$

where the normalization factors and $[2(E+M)(E'+M)]^{-1/2}$ on the right-hand side will be finally resumed. To emphasize dependence on the azimuthal angles φ for $\mathbf{p}_\perp$, φ' for $\mathbf{p}'_\perp$, and φ_k for $\mathbf{k}_\perp$, we denote

$$F^{\mathrm{P}}(\varphi,\varphi',\varphi_k)=a^\dagger_{\kappa_\gamma\ell_\gamma}(\mathbf{k}_\perp)a^\dagger_{\kappa'\ell'}(\mathbf{p}'_\perp)a_{\kappa\ell}(\mathbf{p}_\perp)(\mathcal{A}^{\mathrm{P}}_{0n}+M\xi\mathcal{A}^{\mathrm{P}}_{1n}). \tag{43}$$

Now we work out the integrals over the three transverse momenta.

1. Transverse integrals excluding φ

The integral over the magnitude of each transverse momentum is trivially finished by the δ function of the Bessel vortex. The planar integrals over any two of the three azimuthal angles, say, φ', φ_k, with the constraint of transverse momentum conservation are accomplished in Appendix B. The result is,

$$S_{\mathrm{B}}^{\mathrm{P}} = -ie\sum_{n=n_0}^{\infty}(2\pi)^4 2\delta(u_n\Omega^- + P^-)\delta(P^+) \times\int\frac{p_\perp dp_\perp}{(2\pi)^2}\int\frac{p'_\perp dp_\perp}{(2\pi)^2}\int\frac{k_\perp dk_\perp}{(2\pi)^2}\frac{1}{2\Delta} \times\int d\varphi\sum_{\eta=\pm}F^{\mathrm{P}}(\varphi,\varphi'_\eta,\varphi_{k\eta}), \tag{44}$$

where $\eta=\pm$ denotes the two solutions to the constraint on three transverse momenta of fixed magnitudes, and

$$\Delta=\frac{1}{4}\sqrt{-\lambda(p_\perp^2,p_\perp'^2,k_\perp^2)}, \tag{45a}$$

$$\varphi'_\eta=\varphi-\eta\delta', \quad \varphi_{k\eta}=\varphi+\eta\delta_k, \tag{45b}$$

$$\angle(\mathbf{p}_\perp,\mathbf{p}'_\perp)=\delta'=\arccos\frac{p_\perp^2+p_\perp'^2-k_\perp^2}{2p_\perp p'_\perp}, \tag{45c}$$

$$\angle(\mathbf{p}_\perp,\mathbf{k}_\perp)=\delta_k=\arccos\frac{p_\perp^2+k_\perp^2-p_\perp'^2}{2p_\perp k_\perp}, \tag{45d}$$

where we used the standard triangular function $\lambda(a,b,c)=a^2+b^2+c^2-2ab-2bc-2ca$.

2. Integrals over φ

Inspecting the form of $F^{\mathrm{P}}(\varphi,\varphi'_\eta,\varphi_{k\eta})$, we see that there are three sources of φ dependence. First, the kernel of the Bessel vortex for all three states offers the phase factor:

$$e^{i(\ell\varphi-\ell'\varphi'_\eta-\ell_\gamma\varphi_{k\eta})}=e^{i\varphi\Delta\ell}e^{i\eta(\ell'\delta'-\ell_\gamma\delta_k)}, \quad \Delta\ell=\ell-\ell'-\ell_\gamma. \tag{46}$$

The second source of φ enters through the variable τ_ρ. For a circularly polarized laser τ_ρ appears as a phase $\exp(in\tau_\rho)$, while for a linearly polarized laser it appears as an argument $\gamma^{\mathrm{L}}=\sqrt{2}\gamma^{\mathrm{C}}\cos\tau_\rho$ of the Bessel function. Note that $\gamma^{\mathrm{C}}\propto\rho$ does not involve φ. We compute

$$\rho^2=\frac{k_+^2p_\perp^2}{p_+^4}+\frac{k_\perp^2}{p_+^2}-\frac{k_+(p_\perp^2+k_\perp^2-p_\perp'^2)}{p_+^3}, \tag{47a}$$

$$\rho\cos\tau_\rho=\rho\cos(\varphi-\eta\varphi_0), \quad \rho\sin\tau_\rho=\rho\sin(\varphi-\eta\varphi_0), \tag{47b}$$

i.e., $\tau_\rho = \varphi - \eta\varphi_0$, where φ_0 is determined by

$$\frac{k_+ p_\perp}{p_+^2} - \frac{k_\perp \cos\delta_k}{p_+} = \rho\cos\varphi_0,$$
$$\frac{k_\perp}{p_+}\sin\delta_k = \rho\sin\varphi_0. \tag{48}$$

Finally, φ appears as a polynomial of triangular functions in the $B_{0,1}$ functions, which involve φ through the following variables:

$$r_\lambda = \frac{k_\perp}{k_+}e^{-i\lambda(\varphi+\eta\delta_k)}, \quad p_\sigma = p_\perp e^{i\sigma\varphi}, \tag{49a}$$

$$p'_\sigma = p'_\perp e^{i\sigma(\varphi-\eta\delta')}, \quad p'_{\bar\sigma} = p'_\perp e^{-i\sigma(\varphi-\eta\delta')}. \tag{49b}$$

Note that $R^3 = \eta p_\perp p'_\perp \sin\delta'$ and $2\mathbf{p}'_\perp\cdot\mathbf{p}_\perp = p_\perp^2 + p_\perp'^2 - k_\perp^2$ do not depend on azimuthal angles.

Now we collect the above sources of φ dependence and finish the φ integrals. For a circularly polarized laser, this is trivial and yields Kronecker δ's involving various combinations of $\Delta\ell$, n, λ, σ, and $\sigma' = \pm\sigma$. This reflects the axial symmetry of the process around the laser propagation direction. Suppressing the following factors on the right-hand side,

$$i^{-\Delta\ell}e^{i\eta(\ell'\delta'-\ell_\gamma\delta_k)}\frac{1}{\sqrt{2(E+M)(E'+M)}}$$
$$\times\sqrt{\frac{2\pi}{\kappa}\frac{2\pi}{\kappa'}\frac{2\pi}{\kappa_\gamma}}\delta(p_\perp-\kappa)\delta(p'_\perp-\kappa')\delta(k_\perp-\kappa_\gamma), \tag{50}$$

we have

$$\int d\varphi\, F^{\mathrm{C}}(\varphi,\varphi'_\eta,\varphi_{k\eta})$$
$$= \int d\varphi\, e^{i\Delta\ell\varphi}\left[B_0 J_n(\gamma^{\mathrm{C}})e^{in\tau_\rho} + \frac{M\xi}{\sqrt{2}}B_1 J_{n-\lambda}(\gamma^{\mathrm{C}})e^{i(n-\lambda)\tau_\rho}\right]$$
$$= (0_{\mathrm{s}}^{\mathrm{C}})J_n(\gamma^{\mathrm{C}}) + (1_{\mathrm{s}}^{\mathrm{C}})\frac{M\xi}{\sqrt{2}}J_{n-\lambda}(\gamma^{\mathrm{C}}), \tag{51}$$

where the subscript $\mathrm{s} = \mathrm{p}, \mathrm{f}$ denotes the electron spin-preserved ($\sigma' = \sigma$) and -flipped ($\sigma' = \bar\sigma = -\sigma$) cases. For the spin-preserved case,

$$(0_{\mathrm{p}}^{\mathrm{C}}) = (0_{\mathrm{p}})e^{i(\Delta\ell-\lambda)\eta\varphi_0}\delta_{\Delta\ell+n-\lambda,0}, \tag{52a}$$

$$(1_{\mathrm{p}}^{\mathrm{C}}) = (1_{\mathrm{p}})e^{i\Delta\ell\eta\varphi_0}\delta_{\Delta\ell+n-\lambda,0}, \tag{52b}$$

where

$$(0_{\mathrm{p}}) = [(p'_+ + M)(p_+ + M) + (\mathbf{p}'_\perp\cdot\mathbf{p}_\perp + iR^3\sigma)]\frac{k_\perp}{k_+}e^{-i\lambda\eta\delta_k}$$
$$-[2\delta_{\lambda\bar\sigma}(E'+M)p_\perp + 2\delta_{\lambda\sigma}(E+M)p'_\perp e^{i\lambda\eta\delta'}], \tag{53a}$$

$$(1_{\mathrm{p}}) = +\left(\frac{\delta_{\lambda\sigma}}{p'_+}+\frac{\delta_{\lambda\bar\sigma}}{p_+}\right)(p'_+ + M)(p_+ + M)$$
$$+\left(\frac{\delta_{\lambda\bar\sigma}}{p'_+}+\frac{\delta_{\lambda\sigma}}{p_+}\right)(\mathbf{p}'_\perp\cdot\mathbf{p}_\perp + i\sigma R^3), \tag{53b}$$

and for the spin-flipped case,

$$(0_{\mathrm{f}}^{\mathrm{C}}) = (0_{\mathrm{f}})e^{in(-\eta\varphi_0)}\delta_{\Delta\ell+n-\lambda+\sigma,0}, \tag{54a}$$

$$(1_{\mathrm{f}}^{\mathrm{C}}) = (1_{\mathrm{f}})e^{i(\Delta\ell+\sigma)\eta\varphi_0}\delta_{\Delta\ell+n-\lambda+\sigma,0}, \tag{54b}$$

where

$$(0_{\mathrm{f}}) = \sigma\Big\{\frac{k_\perp}{k_+}[(p_+ + M)p'_\perp e^{-i\sigma\eta\delta'} - (p'_+ + M)p_\perp]e^{-i\lambda\eta\delta_k}$$
$$+2\delta_{\lambda\sigma}[(p_+ + M)p'^3 - (p'_+ + M)p^3]\Big\}, \tag{55a}$$

$$(1_{\mathrm{f}}) = \sigma\Big\{\left(\frac{\delta_{\lambda\sigma}}{p'_+}+\frac{\delta_{\lambda\bar\sigma}}{p_+}\right)(p_+ + M)p'_\perp e^{-i\sigma\eta\delta'}$$
$$-\left(\frac{\delta_{\lambda\bar\sigma}}{p'_+}+\frac{\delta_{\lambda\sigma}}{p_+}\right)(p'_+ + M)p_\perp\Big\}. \tag{55b}$$

The φ integrals are more involved in the case of a linearly polarized laser in which the argument of the Bessel function in integrands contains φ. But they are still integrable since only a single Bessel function is multiplied by an integral phase of φ. We show the calculation details of the basic integral G in Appendix C. Suppressing again the same factors as in Eq. (50), we have

$$\int d\varphi F^{\mathrm{L}}(\varphi,\varphi'_\eta,\varphi_{k\eta})$$
$$= \sum_{\nu=-\infty}^{\infty}J_\nu(\beta)\int d\varphi e^{i\Delta\ell\varphi}\Big[B_0 J_{2\nu+n}(\gamma^{\mathrm{L}})$$
$$+\frac{M\xi}{2}B_1(J_{2\nu+n-1}(\gamma^{\mathrm{L}}) + J_{2\nu+n+1}(\gamma^{\mathrm{L}}))\Big]$$
$$= \sum_{\nu=-\infty}^{\infty}\left[(0_{\mathrm{s}}^{\mathrm{L}}) + \frac{M\xi}{2}(1_{\mathrm{s}}^{\mathrm{L}})\right]J_\nu(\beta), \tag{56}$$

where for the electron spin-preserved case,

$$(0_{\mathrm{p}}^{\mathrm{L}}) = (0_{\mathrm{p}})G^{\Delta\ell-\lambda}_{2\nu+n}(\eta), \tag{57a}$$

$$(1_{\mathrm{p}}^{\mathrm{L}}) = (1_{\mathrm{p}})\big[G^{\Delta\ell}_{2\nu+n-1}(\eta) + G^{\Delta\ell}_{2\nu+n+1}(\eta)\big], \tag{57b}$$

and for the spin-flipped case,

$$(0_{\mathrm{f}}^{\mathrm{L}}) = (0_{\mathrm{f}})G^{\Delta\ell+\sigma-\lambda}_{2\nu+n}(\eta), \tag{58a}$$

$$(1_{\mathrm{f}}^{\mathrm{L}}) = (1_{\mathrm{f}})\big[G^{\Delta\ell+\sigma}_{2\nu+n-1}(\eta) + G^{\Delta\ell+\sigma}_{2\nu+n+1}(\eta)\big]. \tag{58b}$$

Since the nonvanishing of $G^m_\mu(\eta)$ demands the same parity of the integers μ, m, the following integers are even in their respective cases: $n+\Delta\ell-\lambda$ for $(0^{\rm L}_{\rm p})$, $n+\Delta\ell\pm1$ for $(1^{\rm L}_{\rm p})$, $n+\Delta\ell+\sigma-\lambda$ for $(0^{\rm L}_{\rm f})$, and $n+\Delta\ell+\sigma\pm1$ for $(1^{\rm L}_{\rm f})$. Since $\lambda=\pm1$ and $\sigma=\pm1$, this translates into the statement that n has opposite parity to $\Delta\ell$ for the electron spin-preserved case and the same parity as $\Delta\ell$ for the spin-flipped case.

3. Bessel-vortex amplitude

For bookkeeping purposes we write down the scattering matrix element by collecting all factors except for the normalization factors of the initial and final states:

$$S^{\rm P}_{\rm B}=(-ie)i^{-\Delta\ell}\sqrt{\frac{\kappa}{2\pi}\frac{\kappa'}{2\pi}\frac{\kappa_\gamma}{2\pi}}\frac{1}{\sqrt{2(E+M)(E'+M)}}\times\frac{1}{2\Delta}(2\pi)\delta(P_+)\sum_{n=n_0}^{\infty}2\delta(u_n\Omega_-+P_-)\Upsilon^{\rm P}_n, \tag{59}$$

where

$$\Upsilon^{\rm P}_n=\sum_{\eta=\pm}e^{i\eta(\ell'\delta'-\ell_\gamma\delta_k)}\times\begin{cases}(0^{\rm C}_{\rm s})J_n(\gamma^{\rm C})+(1^{\rm C}_{\rm s})\frac{M\xi}{\sqrt{2}}J_{n-\lambda}(\gamma^{\rm C}), & {\rm P=C},\\ \sum_{\nu=-\infty}^{\infty}\left[(0^{\rm L}_{\rm s})+\frac{M\xi}{2}(1^{\rm L}_{\rm s})\right]J_\nu(\beta), & {\rm P=L},\end{cases} \tag{60}$$

and $p_\perp=\kappa, p'_\perp=\kappa', k_\perp=\kappa_\gamma$ are implied on the right-hand side. We recall some features related to the laser polarization. For the circular polarization, only one Bessel function is involved in each term, and for given $\Delta\ell,\sigma,\sigma',\lambda$ only one n actually contributes ($n=\lambda-\Delta\ell>0$ for the electron spin-preserved case and $n=\lambda-\Delta\ell-\sigma>0$ for the electron spin-flipped case). This is again a result of angular momentum conservation in the z direction. The initial electron has its angular momentum component in the z direction, $\ell+\sigma/2$, and the absorbed $n>0$ laser photons contribute n; the final electron has $\ell'+\sigma'/2$, and the radiated photon has $\ell_\gamma+\lambda$. Conservation of the angular momentum component gives $\Delta\ell+n=\lambda+(\sigma'-\sigma)/2$ which yields the Kronecker δ. Since $n>0$, $\Delta\ell$ tends to be negative. In the case of the linear polarization without the axial symmetry, each term is a product of three Bessel functions, and there are double infinite sums over n and ν. Considering its simplicity our numerical analysis focuses mainly on the case of a circularly polarized laser.

D. Amplitude squared and decay rate for vortex electrons and photon

1. Case for Bessel vortex

On taking the absolute square of $S^{\rm P}_{\rm B}$ in Eq. (59), we first cope with the sum over n and the squaring of the δ functions. Given a point in the final-state phase space of $\mathbf{p}',\mathbf{k}'$, the argument of $\delta(u_n\Omega_-+P_-)$ being linear in n can vanish for at most one value of n. There is thus no interference between different n terms. This is consistent with the physical interpretation that n may be understood as the net number of laser photons involved in the process. Now consider the square of δ functions. The one involving the conserved plus component of momentum is,

$$2\pi\delta(P_+)=\int\frac{1}{2}dx_-\exp\left(\frac{i}{2}x_-P_+\right)\Rightarrow[2\pi\delta(P_+)]^2=2\pi\delta(P_+)\frac{L_-}{2}. \tag{61}$$

More care must be taken for $[\delta(u_n\Omega_-+P_-)]^2$. The variable u was introduced as an auxiliary parameter to uniformize momentum conservation among all components in the presence of a plane-wave laser. To proceed in a clear manner, we go back to the original u and τ integrals in Sec. II B 2. Finishing first the τ (u) integral and then the u (τ) integral yields the first (second) equality respectively:

$$\int d\tau\int du\,\delta(u\Omega_-+P_-)e^{i(u+2\beta-n)\tau}=2\pi\delta(u_n\Omega_-+P_-)=\frac{1}{\Omega_-}2\pi\delta(u+2\beta-n)|_{u=-P_-/\Omega_-}. \tag{62}$$

Squaring the above gives

$$\begin{aligned}[2\pi\delta(u_n\Omega_-+P_-)]^2&=\frac{1}{\Omega_-^2}[2\pi\delta(u+2\beta-n)|_{u=-P_-/\Omega_-}]^2\\&=\frac{1}{\Omega_-^2}2\pi\delta(u+2\beta-n)|_{u=-P_-/\Omega_-}\int d\tau e^{i0\cdot\tau}\\&=2\pi\delta(u_n\Omega_-+P_-)\frac{L_+}{2}.\end{aligned} \tag{63}$$

The amplitude squared is thus

$$|S^{\rm P}_{\rm B}|^2=e^2\frac{\kappa}{2\pi}\frac{\kappa'}{2\pi}\frac{\kappa_\gamma}{2\pi}\frac{1}{2(E+M)(E'+M)}\frac{1}{(2\Delta)^2}2\pi\delta(P_+)\times\frac{L_-}{2}\frac{L_+}{2}\frac{2}{\pi}\sum_{n=n_0}^{\infty}\delta(u_n\Omega_-+P_-)|\Upsilon^{\rm P}_n|^2. \tag{64}$$

Since the laser background has been completely taken into account in the initial and final electron states, we are actually coping with a single dressed electron in the initial state. In this circumstance, it is more appropriate to consider the process as the decay of a dressed electron into another dressed electron and a photon. We thus compute its decay rate which has the usual meaning of

the number of decays per unit time per particle. Multiplying $|S_{\rm B}^{\rm P}|^2$ by normalization factors and number densities of final-state particles and dividing it by the time L_+, we obtain the decay rate [100]:

$$d\Gamma_{\rm B}^{\rm P} = \frac{|S_{\rm B}^{\rm P}|^2}{L_+}(N_p^{\rm B})^2 \frac{d\kappa' dp'_+}{2p'_+ 2\pi}\frac{d\kappa_\gamma dk_+}{2k_+ 2\pi}$$
$$= e^2 \frac{\kappa}{2\pi}\frac{\kappa'}{2\pi}\frac{\kappa_\gamma}{2\pi}\frac{1}{2(E+M)(E'+M)}\frac{1}{2\Delta^2}\frac{\pi}{R}\frac{1}{2p_+}\delta(P_+)$$
$$\times \sum_{n=n_0}^{\infty}\delta(u_n\Omega_- + P_-)|\Upsilon_n^{\rm P}|^2 \frac{d\kappa' dp'_+}{2p'_+ 2\pi}\frac{d\kappa_\gamma dk_+}{2k_+ 2\pi}. \quad (65)$$

The presence of the awkward factor $1/R$ in the above signifies the non-normalizability of the Bessel vortex in the transverse plane. Now we employ the Bessel-Gaussian vortex to normalize the initial electron.

2. Modifications for an initial Bessel-Gaussian vortex electron

The above result for the decay rate is singular at $\Delta = 0$ when the triangle formed by the three transverse momenta $\mathbf{p}_\perp = \mathbf{p}'_\perp + \mathbf{k}_\perp$ shrinks to a line. This singularity of order Δ^{-2} in the rate is not integrable [89,97]. Now we show that it can be made integrable by employing a Gaussian-smeared Bessel-Volkov vortex for the initial electron, so that the rate becomes a measurable quantity. Since such a vortex is a linear composition of the Bessel-Volkov solution to the Dirac equation which by itself is also linear, it is still a solution. But it is not unique to compose the solution. As we argued previously, it is more natural to employ light-front coordinates in the presence of a plane-wave laser. We therefore propose to work with a Gaussian vortex of fixed plus momentum, Eq. (13).

There are two modifications to the first equality for the decay rate in Eq. (65). First, the normalization factor $N_p^{\rm B}$ for the initial electron should be replaced by $N_p^{\rm BG}$ in Eq. (19), which effectively removes the factor π/R while keeping $1/(2p_+)$ in the second equality of Eq. (65). Second, the S matrix element $S_{\rm B}^{\rm P}$ in Eq. (59) should be weighted by the Gaussian function in Eq. (14) and integrated over κ to become the S matrix element $S_{\rm BG}^{\rm P}$, as we detail below.

Let us enumerate all κ dependence other than the Gaussian function in $S_{\rm B}^{\rm P}$. First, the trivial square root factors. Second, $\delta(u_n\Omega_- + P_-)$ depends on κ through p_- in P_-. Since $p_+\delta p_- - 2\kappa\delta\kappa = 0$ for an on-shell electron with fixed p_+, $\delta p_- \ll \delta\kappa$ for $\kappa \ll p_+$ which is the vortex that can be practically realized. Note β in $u_n = n - 2\beta$ is independent of κ; see Eq. (33a). That there are two solutions to n on varying κ requires at least $\kappa\delta\kappa \geq \omega p_+$. Considering further the Gaussian suppression for κ deviating from its central value, the effect due to κ variation must be tiny. Neglecting it there will be no interference between different n terms when squaring $S_{\rm B}^{\rm P}$ as is the case with pure Bessel-vortex states. The third source of κ dependence is $\Upsilon_n^{\rm P}$, Eq. (60). The good news is that the argument $\gamma^{\rm C}$ in Eq. (33a) of the Bessel function in the case of a circularly polarized laser is independent of κ. This is because the magnitude ρ is actually independent of transverse momenta although its definition as a vector in Eq. (33b) involves them. We verify this as follows. By definition,

$$\vec{\rho}^2 = \frac{k_+^2}{p_+^4}p_\perp^2 + \frac{k_\perp^2}{p_+^2} - \frac{k_+}{p_+^3}2\mathbf{k}_\perp\cdot\mathbf{p}_\perp. \quad (66)$$

Using $2k\cdot p = k_+p_- + k_-p_+ - 2\mathbf{k}_\perp\cdot\mathbf{p}_\perp$ and on-shell conditions $p_\perp^2 = p_+p_- - M^2$ and $k_\perp^2 = k_+k_-$ to replace all scalar products of transverse momenta, the above becomes

$$\vec{\rho}^2 = \frac{k_+}{p_+^3}2k\cdot p - \frac{k_+^2}{p_+^4}M^2. \quad (67)$$

Identifying u in Eq. (30) with u_n through the δ function, we have $2k\cdot p = u_n 2p'_+\omega$, so that

$$\vec{\rho}^2 = \frac{k_+}{p_+^3}u_n 2p'_+\omega - \frac{k_+^2}{p_+^4}M^2, \quad (68)$$

which is independent of transverse momenta as claimed. In the case of a linearly polarized laser, as we show in Appendix C this only brings in integral phases of φ_0 as in the case of circular polarization. The remaining κ dependence in $\Upsilon_n^{\rm P}$ appears in the form of polynomials in κ, E, p_- and in the form of integer phases of δ', δ_k.

All κ dependence mentioned above is smooth. The only apparently singular behavior enters through the factor Δ^{-1}, which we now turn to discuss. To simplify notations, we use the variables

$$x = \kappa, \quad b = \kappa', \quad c = \kappa_\gamma. \quad (69)$$

Given a point in the final-state phase space, that the transverse momenta form a triangle demands

$$x_1 \leq x \leq x_2, \quad x_1 = |b-c|, \quad x_2 = b+c. \quad (70)$$

The factor Δ^{-1} introduces apparent singularities at the delimiters of the integral over $\kappa = x$:

$$\Delta = \frac{1}{4}\sqrt{(x+x_1)(x+x_2)}\sqrt{(x_2-x)(x-x_1)}. \quad (71)$$

The scattering matrix element $S_{\rm B}^{\rm P}$ in Eq. (59) is replaced by

$$S_{\rm BG}^{\rm P} = (-ie)i^{-\Delta\ell}(2\pi)\delta(P_+)\sum_{n=n_0}^{\infty}2\delta(u_n\Omega_- + P_-)I_{\rm BG}^{\rm P}, \quad (72)$$

where

$$I^{\rm P}_{\rm BG} = \int_{x_1}^{x_2} dx \frac{g(x)}{\sqrt{(x_2-x)(x-x_1)}}, \tag{73a}$$

$$g(x) = \frac{2f(x;\kappa_0,\sigma_\perp)}{\sqrt{(x+x_1)(x+x_2)}} \times \left[\sqrt{\frac{\kappa}{2\pi}\frac{\kappa'}{2\pi}\frac{\kappa_\gamma}{2\pi}}\frac{e^{i\eta(\ell'\delta'-\ell_\gamma\delta_k)}}{\sqrt{2(E+M)(E'+M)}}\Upsilon^{\rm P}_n\right]_{\kappa=x}. \tag{73b}$$

We have set κ in $\delta(u_n\Omega_- + P_-)$ to its central value κ_0, i.e., $p_- = (M^2+\kappa_0^2)/p_+$, and included in the function $g(x)$ all smooth dependence of κ and the Gaussian function. The integral $I_{\rm BG}$ is manipulated in Appendix D into a form that involves no apparent singularities and is amenable to numerical computation. The decay rate is,

$$\begin{aligned} d\Gamma^{\rm P}_{\rm BG} &= \frac{|S^{\rm P}_{\rm BG}|^2}{L_+}(N^{\rm BG}_p)^2\frac{d\kappa' dp'_+}{2p'_+2\pi}\frac{d\kappa_\gamma dk_+}{2k_+2\pi} \\ &= e^2 2\delta(P_+)\sum_{n=n_0}^{\infty}\delta(u_n\Omega_- + P_-)|I^{\rm P}_{\rm BG}|^2 \\ &\quad\times\frac{1}{2p_+}\frac{d\kappa' dp'_+}{2p'_+2\pi}\frac{d\kappa_\gamma dk_+}{2k_+2\pi}. \end{aligned} \tag{74}$$

The κ' and p'_+ integrals are finished by the two δ functions, i.e.,

$$p'_+ = E(1+v\cos\theta_p) - \omega_\gamma(1+\cos\theta_\gamma), \tag{75a}$$

$$\begin{aligned} \kappa'^2 &= \kappa^2 + \omega_\gamma^2\sin^2\theta_\gamma + 2n\omega[E(1+v\cos\theta_p) \\ &\quad - \omega_\gamma(1+\cos\theta_\gamma)] - 2\omega E(1-v\cos\theta_p\cos\theta_\gamma) \\ &\quad - \frac{1}{2}M^2\xi^2\frac{\omega_\gamma(1+\cos\theta_\gamma)}{E(1+v\cos\theta_p)}, \end{aligned} \tag{75b}$$

where v is the magnitude of the velocity of the initial electron. For the emitted vortex photon, we employ its angular frequency ω_γ and opening angle θ_γ to characterize its kinematical distributions by the relation, $dk_+ d\kappa_\gamma = \omega_\gamma(1+\cos\theta_\gamma)d\omega_\gamma d\theta_\gamma$. With all of the above manipulations, the two-dimensional differential decay rate in terms of the emitted photon's variables becomes,

$$d\Gamma^{\rm P}_{\rm BG} = \frac{e^2}{32\pi^2 E(1+v\cos\theta_p)}\sum_{n=n_0}^{\infty}\frac{|I^{\rm P}_{\rm BG}|^2}{\kappa'}d\omega_\gamma d\theta_\gamma. \tag{76}$$

Given the variables (E,θ_p,v) of the initial electron and the laser's angular frequency ω and parameter ξ, the angular frequency of the emitted vortex photon is bound by $\omega_- \le \omega_\gamma \le \omega_+$ for a given θ_γ, where

$$\omega_\pm = \frac{n\omega E(1+v\cos\theta_p)}{E[1-v\cos(\theta_\gamma \mp \theta_p)] + \{n\omega + M^2\xi^2/[4E(1+v\cos\theta_p)]\}(1+\cos\theta_\gamma)}. \tag{77}$$

Note that at $\theta_\gamma = \pi$ $\omega_\pm$ coincide and are equal to $n\omega$.

Before embarking on numerical analysis we discuss briefly an alternative treatment of final-state particles. In the present work, we assume that the final electron and γ photon are in a Bessel state, i.e., we assume the detection of vortex particles after scattering. We note that, applying the technique of evolved states studied in Ref. [101] offers an alternative way of dealing with the process, i.e., by calculating first the evolved state in a complete basis set of the plane-wave solutions and then analyzing the angular momentum projection. However, by summing over the contributions of all possible Bessel states of the final electron and γ photon, our result agrees with that of the plane-wave final electron and γ photon. Thus these two methods should be equivalent. This is in agreement with the discussion in Ref. [89].

III. NUMERICAL ANALYSIS

In this section we evaluate numerically the rate for all-vortex nonlinear Compton scattering based on the analytical result in Sec. II. We focus mainly on the case of a circularly polarized laser, and discuss briefly the case of a linearly polarized laser. For the laser parameters, we assume its angular frequency $\omega = 1$ eV and dimensionless intensity $\xi = 0.1, 1, 5$. This corresponds to a laser intensity in the range from 2×10^{16} to 5×10^{19} W/cm^2, which can be achieved in current experiments [102]. We assume that the initial electron has an energy $E = 1$ GeV which could be obtained by accelerating a low-energy vortex electron to higher energy [86]. Unless otherwise stated, we assume its Bessel-Gaussian vortex has a deviation $\sigma_\perp$ of one percent of its central value κ_0, $\sigma_\perp = 0.01\kappa_0$. We recall that angular momentum is conserved in the longitudinal direction for a circularly polarized laser [see Eq. (51)], which results in the constraint $\Delta\ell + n - \lambda = 0$ for the electron spin-preserved channel and $\Delta\ell + n - \lambda + \sigma = 0$ for the electron spin-flipped channel. There is no such a conservation law in the case of a linearly polarized laser, and hence we have to sum up the contributions from all possible harmonic numbers.

A. Circularly polarized laser with $\xi = 0.1$

1. The electron spin-preserved case

We start with the case when the electron preserves its spin $\sigma' = \sigma$ upon colliding against a less intense laser with

$\xi = 0.1$. The exchanges of angular momenta among the electron, photon, and laser are discussed, by analyzing a number of combinations of the topological charges of the initial vortex electron ℓ, the final vortex electron ℓ', and the emitted vortex photon ℓ_γ. The impact of the opening angle θ_p of the initial electron is also analyzed.

In Fig. 2 we depict the spectrum $d\Gamma_{\ell\ell'\ell_\gamma}/d\omega_\gamma$ of the emitted vortex photon for the case of $\ell = \ell' = 10$ and $\sigma = \sigma' = +1$. Our analysis shows that the case with $\sigma = \sigma' = -1$ is very similar. Two values of the opening angle of the initial electron $\theta_p = 1$ mrad and $\theta_p = 0.1$ rad are considered. The spectrum $d\Gamma_{\ell\ell'\ell_\gamma}/d\omega_\gamma$ is obtained by finishing the opening angle θ_γ integral in the two-dimensional distribution $d\Gamma_{\ell\ell'\ell_\gamma}/(d\omega_\gamma d\theta_\gamma)$. The emitted photon's ℓ_γ is restricted by the angular momentum conservation $\ell_\gamma = \ell - \ell' + n - \lambda$, as discussed above. For a given ℓ_γ, its energy lies between $n\omega$ and ω_+, as can be clearly seen in Fig. 2. While the maximum energy of the emitted photon increases with its ℓ_γ, the rate $d\Gamma_{\ell\ell'\ell_\gamma}/d\omega_\gamma$ decreases by a few orders of magnitude. The combination of these two factors offers a chance to separate the emitted vortex γ photons with different ℓ_γ; namely, in every given

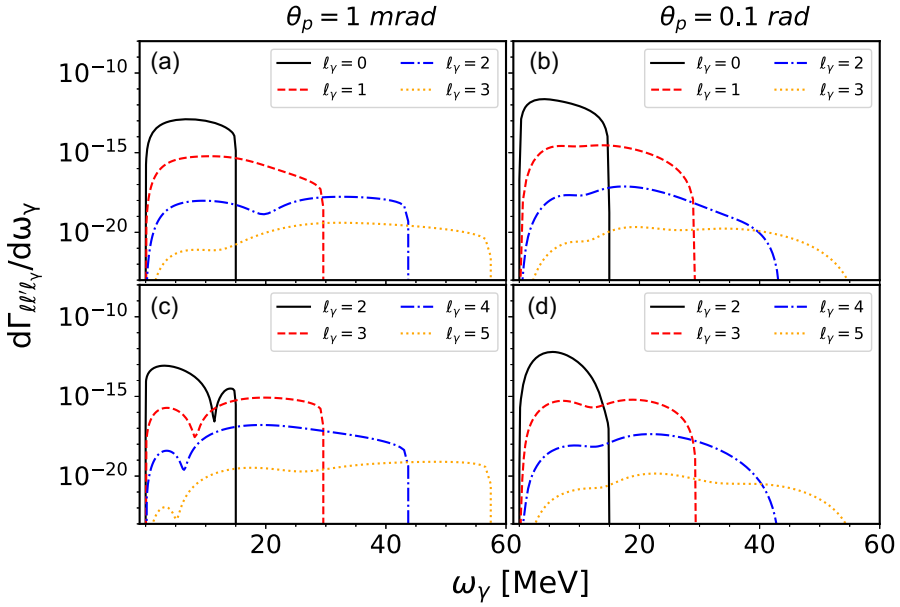


FIG. 2. The distribution $d\Gamma_{\ell\ell'\ell_\gamma}/d\omega_\gamma$ of the emitted vortex γ photon at $\theta_p = 1$ mrad ($\theta_p = 0.1$ rad) is shown in panels (a) and (c) [(b) and (d)], and for the photon helicity $\lambda = +1$ ($\lambda = -1$) in panels (a) and (b) [(c) and (d)]. In all panels $\ell = \ell' = 10$, $\sigma = \sigma' = +1$, and $\xi = 0.1$. (a), (b) $\lambda = +1$, (c), (d) $\lambda = -1$.

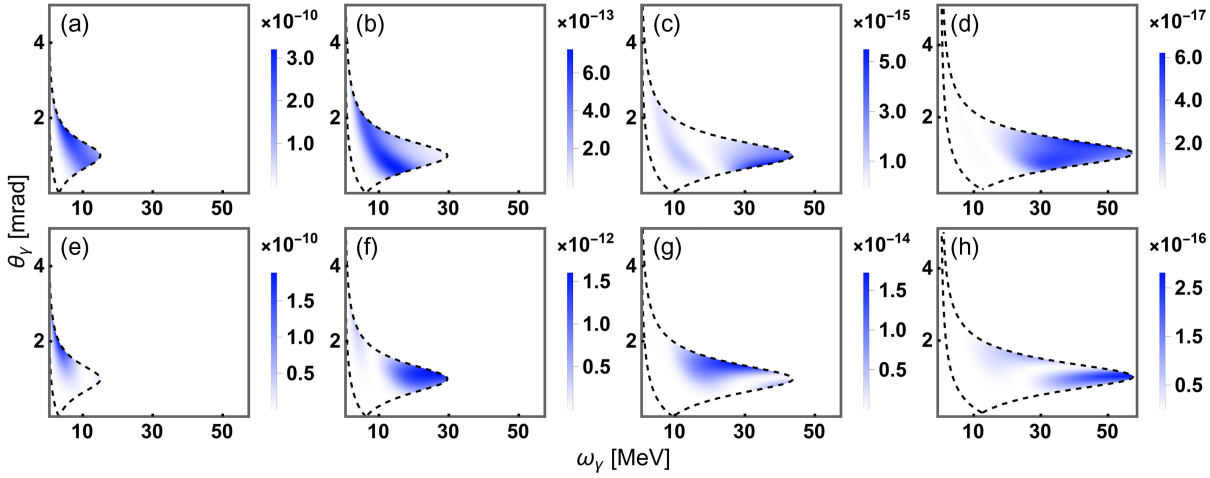


FIG. 3. The two-dimensional distribution $d\Gamma_{\ell\ell'\ell_\gamma}/(d\omega_\gamma d\theta_\gamma)$ for $\lambda = +1$ ($\lambda = -1$) is shown in the upper (lower) panels. In all panels $\ell = \ell' = 10$, $\sigma = \sigma' = +1$, $\theta_p = 1$ mrad, and $\xi = 0.1$. (a) $\ell_\gamma = 0$, $\lambda = +1$, (b) $\ell_\gamma = 1$, $\lambda = +1$, (c) $\ell_\gamma = 2$, $\lambda = +1$, (d) $\ell_\gamma = 3$, $\lambda = +1$, (e) $\ell_\gamma = 2$, $\lambda = -1$, (f) $\ell_\gamma = 3$, $\lambda = -1$, (g) $\ell_\gamma = 4$, $\lambda = -1$, (h) $\ell_\gamma = 5$, $\lambda = -1$.

energy range, one value of ℓ_γ dominates over other values. Furthermore, a double-peak or multipeak structure can be observed in $d\Gamma_{\ell\ell'\ell_\gamma}/d\omega_\gamma$ for a large enough ℓ_γ.

The impact of the opening angle θ_p of the initial vortex electron which represents the effects of its transverse momentum is shown clearly in Fig. 2. Increasing θ_p results in a larger contribution from the terms in Eqs. (53a) and (53b) proportional to transverse momenta in the amplitude. However, as the spin-preserved case is not very sensitive to transverse momenta, the difference in the rates between the two opening angles $\theta_p = 1$ mrad and $\theta_p = 0.1$ rad is not very large compared with the spin-flipped case to be studied later.

We further analyze the two-dimensional decay-rate distribution $d\Gamma_{\ell\ell'\ell_\gamma}/(d\omega_\gamma d\theta_\gamma)$. The results are presented in Fig. 3 for $\theta_p = 1$ mrad and in Fig. 4 for $\theta_p = 0.1$ rad. Again, the case of $\ell = \ell' = 10$ and $\sigma = \sigma' = +1$ is considered here. The region bound by $\omega_\pm$ in Eq. (77) is the one enclosed by a dashed curve. It can be observed in Figs. 3 and 4 that the opening angle θ_γ of the emitted vortex γ photon is located mainly near the value of the opening angle θ_p of the initial vortex electron. For the case of a

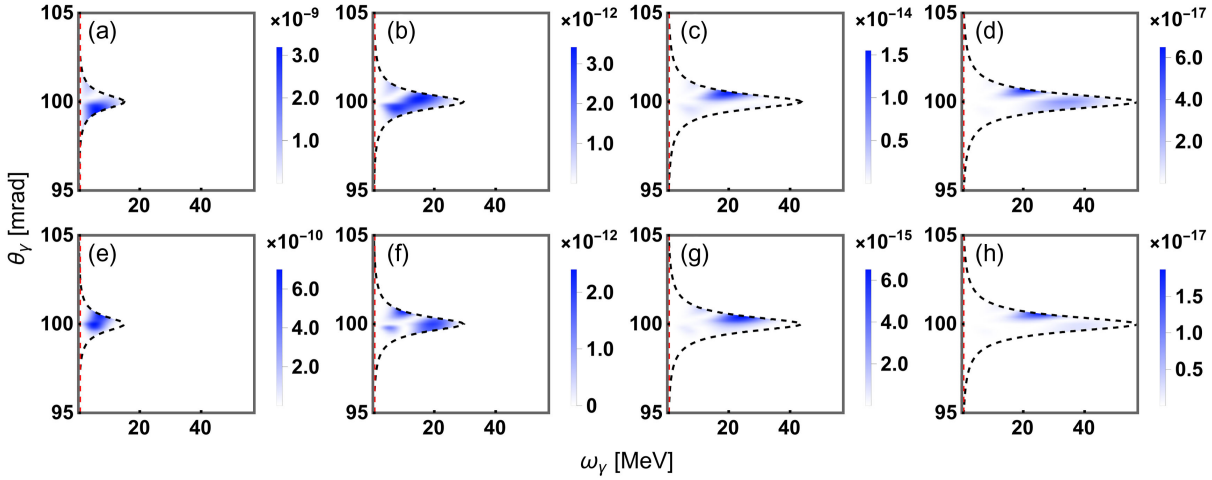


FIG. 4. Same as Fig. 3 except for $\theta_p = 0.1$ rad. (a) $\ell_\gamma = 0$, $\lambda = +1$, (b) $\ell_\gamma = 1$, $\lambda = +1$, (c) $\ell_\gamma = 2$, $\lambda = +1$, (d) $\ell_\gamma = 3$, $\lambda = +1$, (e) $\ell_\gamma = 2$, $\lambda = -1$, (f) $\ell_\gamma = 3$, $\lambda = -1$, (g) $\ell_\gamma = 4$, $\lambda = -1$, (h) $\ell_\gamma = 5$, $\lambda = -1$.

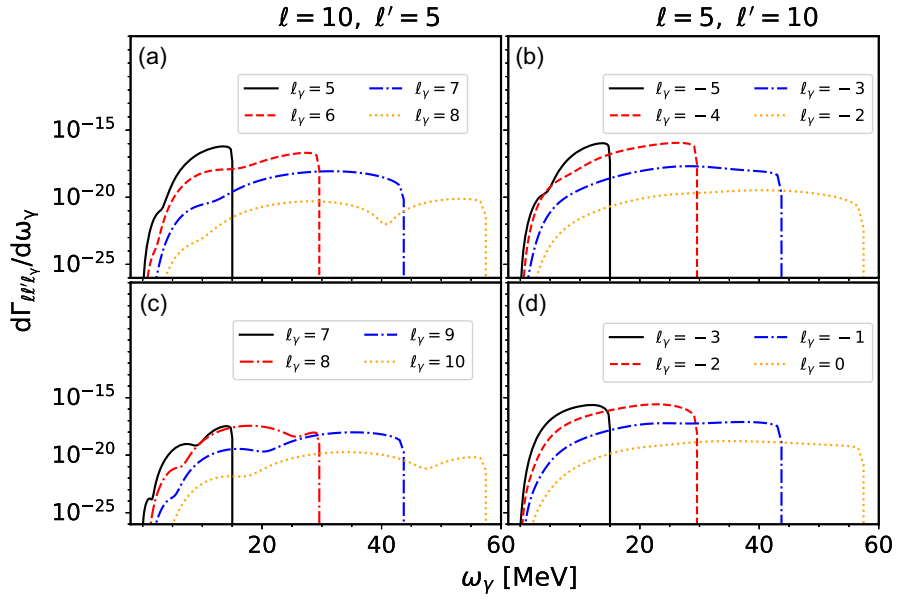


FIG. 5. The distribution $d\Gamma_{\ell\ell'\ell_\gamma}/d\omega_\gamma$ of the emitted vortex γ photon for $\ell = 10, \ell' = 5$ ($\ell = 5, \ell' = 10$) is shown in panels (a) and (c) [(b) and (d)] and $\lambda = +1$ ($\lambda = -1$) in panels (a) and (b) [(c) and (d)], and for various ℓ_γ. In all panels $\sigma = \sigma' = +1$, $\theta_p = 1$ mrad, and $\xi = 0.1$. (a), (b) $\lambda = +1$, (c), (d) $\lambda = -1$.

larger $\theta_p = 0.1$ rad, ω_- is very small which we indicate in Fig. 4 by a red dashed curve.

Now we turn to the case when the topological charge of the final electron is different from that of the initial electron ℓ. The spectrum $d\Gamma_{\ell\ell'\ell_\gamma}/d\omega_\gamma$ of the emitted vortex γ photon is presented in Fig. 5 for the cases $(\ell, \ell') = (10, 5), (5, 10)$. Here we focus on the condition of $\sigma = \sigma' = +1$ and $\theta_p = 1$ mrad. Compared with the results in Fig. 2 with $\ell' = \ell$, the change in the rate with ℓ_γ is not as significant, although the strong ℓ_γ dependence of the maximum energy of the emitted photon still remains. In addition, the feature of $d\Gamma_{\ell\ell'\ell_\gamma}/d\omega_\gamma$ changes from a single-peak structure to a multipeak structure with increasing $|\ell_\gamma|$. This is a combined effect of phases and Bessel functions in the scattering amplitude. For the small opening angle θ_p under consideration here, the photon's transverse momentum $k_\perp$ is much smaller than those of the initial and final electrons $p_\perp$, $p'_\perp$ which thus stay close to each other. Then according to Eqs. (45c) and (45d), δ' is always small while δ_k varies in the whole range from 0 to π making δ_k-dependent phases oscillate rapidly. Those phases enter in the amplitude both as an ℓ_γ-dependent one $e^{-i\ell_\gamma\delta_k}$ and as a helicity-dependent one $e^{-i\lambda\eta\delta_k}$. Furthermore, there are also δ_k-dependent phases that are accompanied by Bessel functions, $e^{-in\eta\varphi_0}J_n(\gamma^C)$ and $e^{-i(n-\lambda)\eta\varphi_0}J_n(\gamma^C)$ where φ_0 depends on δ_k through Eq. (48). The joint effect of all these causes the multipeak structure for a large enough ℓ_γ. This feature can be viewed as a result of the scattering of particles carrying OAMs, and the multipeak structure could help to identify the OAM and spin of the vortex particle.

The comparison of Figs. 2 and 5 also shows that the decay rate is suppressed with increasing $|\ell_\gamma|$ (or $|\ell - \ell'|$ for fixed n, λ). When $|\ell - \ell'|$ or $|\ell_\gamma|$ is sufficiently large, the phase factor oscillates strongly. For Bessel-Gaussian states, this makes the amplitude oscillate strongly, which tends to diminish the integration in Eq. (73a). In fact, $|\ell - \ell'|$ (or $|\ell_\gamma|$) should not be too large as compared with $\kappa_\gamma/\sigma_\perp$ [97], otherwise the decay rate would be very small. For the values of the parameters considered here, the photon transverse momentum κ_γ is indeed not much larger than $\sigma_\perp$, and we therefore see from Fig. 5 the start of the suppression.

2. The electron spin-flipped case

For the electron spin-flipped case with $\sigma' = -\sigma = \pm 1$, we focus on the case of $\ell = \ell' = 10$, and present our results for the opening angle $\theta_p = 1$ mrad of the initial vortex electron in Fig. 6, and for $\theta_p = 0.1$ rad in Fig. 7. A comparison with Fig. 2 shows that the rate for the spin-flipped case is in general smaller by orders of magnitude than the one for the spin-preserved case. This indicates the difficulty in changing and manipulating the electron spin. As shown in Figs. 6(c) and 6(d), there is a symmetry between the cases $\sigma = \lambda = -1$ and $\sigma = \lambda = +1$ when θ_p is small. This is because of the same phase factor and the symmetric form of the dominant terms in the amplitude, Eqs. (55a) and (55b). We observe in Fig. 6 that the rate for the case $\sigma = -\lambda$ [panels (a) and (b)] is much smaller than the case $\sigma = \lambda$ [panels (c) and (d)]. This is because the term $(p^+ + M)p'^3 - (p'^+ + M)p^3$, which is much larger than other terms in the amplitude [see Eq. (55a)] when the opening angle θ_p is small, only contributes for the case $\sigma = \lambda$.

When the opening angle θ_p of the initial vortex electron is larger, the terms proportional to transverse momenta in the amplitude, Eq. (55a), contribute significantly to the rate. This leads to the significant differences between the cases of $\theta_p = 1$ mrad (Fig. 6) and $\theta_p = 0.1$ rad (Fig. 7). When

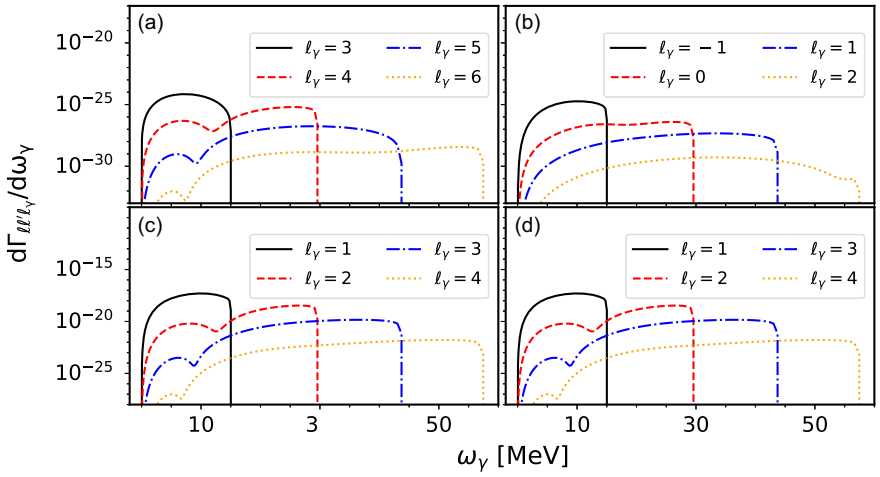


FIG. 6. The distribution $d\Gamma_{\ell\ell'\ell_\gamma}/d\omega_\gamma$ of the emitted vortex γ photon in the electron spin-flipped case: $\sigma' = -\sigma = -1$ ($\sigma' = -\sigma = +1$) in panels (a), (d) [panels (b), (c)] and $\lambda = -1$ ($\lambda = +1$) in panels (a), (c) [panels (b), (d)]. In all panels, $\xi = 0.1$, $\ell = \ell' = 10$, and $\theta_p = 1$ mrad. (a) $\sigma = +1$, $\sigma' = -1$, $\lambda = -1$, (b) $\sigma = -1$, $\sigma' = +1$, $\lambda = +1$, (c) $\sigma = -1$, $\sigma' = +1$, $\lambda = -1$, (d) $\sigma = +1$, $\sigma' = -1$, $\lambda = +1$.

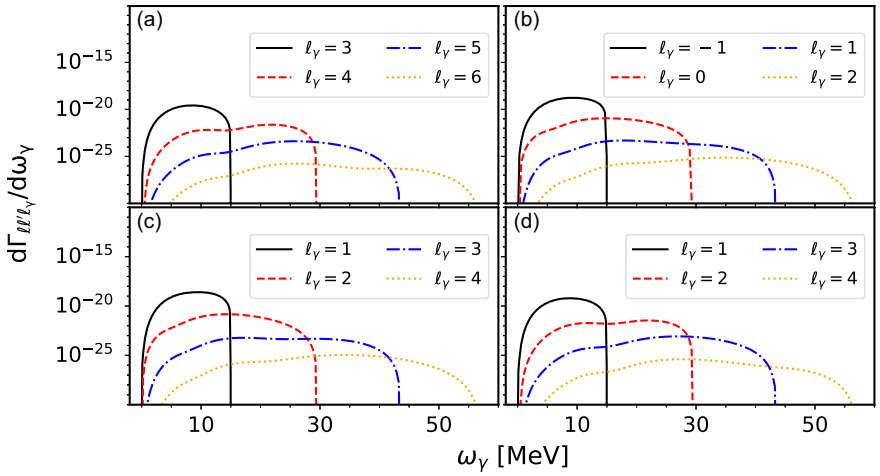


FIG. 7. Same as Fig. 6 except for $\theta_p = 0.1$ rad. (a) $\sigma = +1$, $\sigma' = -1$, $\lambda = -1$, (b) $\sigma = -1$, $\sigma' = +1$, $\lambda = +1$, (c) $\sigma = -1$, $\sigma' = +1$, $\lambda = -1$, (d) $\sigma = +1$, $\sigma' = -1$, $\lambda = +1$.

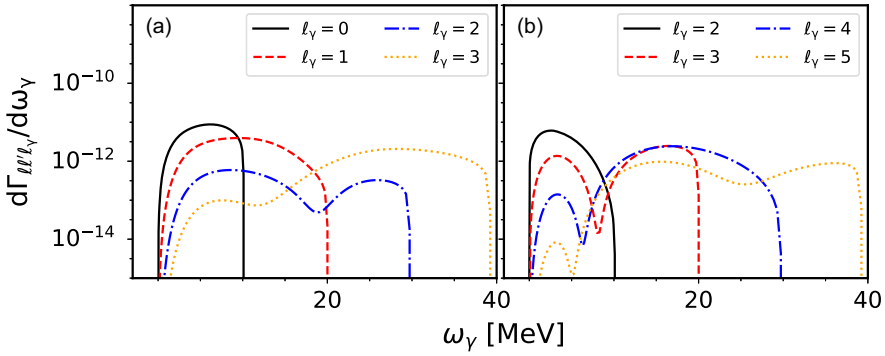


FIG. 8. The distribution $d\Gamma_{\ell\ell'\ell_\gamma}/d\omega_\gamma$ of the emitted vortex γ photon for $\lambda = +1$ ($\lambda = -1$) is shown in panel (a) [panel (b)]. In both panels $\ell = \ell' = 10$, $\theta_p = 1$ mrad, $\sigma = \sigma' = +1$, and $\xi = 1$. (a) $\lambda = +1$, (b) $\lambda = -1$.

θ_p increases from 1 mrad to 0.1 rad, not only does the feature of the photon spectrum change significantly, but also the rate increases by orders of magnitude. This change caused by transverse momenta is especially profound in the case of $\sigma = -\lambda$, since with $\sigma = \lambda$ there still exists the contribution from longitudinal momenta. A comparison with the result in Fig. 2 indicates that the opening angle θ_p has a much stronger impact on the process when the electron flips its spin than when it preserves it. This shows the importance of the opening angle in the coupling between OAM and spin angular momentum, as well as in the manipulation of OAM and spins.

B. Circularly polarized laser with $\xi \geq 1$

Now we investigate the impact of a larger laser intensity by assuming $\xi = 1, 5$, which corresponds to an intensity of about 2×10^{18} and 5×10^{19} W/cm^2 respectively. We continue to work with a small opening angle $\theta_p = 1$ mrad. Since for such a small opening angle the rate in the electron spin-flipped case is much smaller than in the spin-preserved case, we restrict ourselves to the latter, and consider the case $\sigma = \sigma' = +1$. We also assume $\ell = \ell' = 10$.

The spectrum $d\Gamma_{\ell\ell'\ell_\gamma}/d\omega_\gamma$ of the emitted vortex γ photons is presented in Fig. 8 for the case of $\xi = 1$. The rate is much larger than the one with $\xi = 0.1$. Although the rate drops with the increase of ℓ_γ as before, the drop is not as significant as in the case of a smaller intensity parameter $\xi = 0.1$. This has two consequences. On the one hand, it is more difficult to isolate a vortex photon state with a specific ℓ_γ. On the other hand, the emitted photon has a larger average topological charge. We plot the two-dimensional distribution $d\Gamma_{\ell\ell'\ell_\gamma}/(d\omega_\gamma d\theta_\gamma)$ in Fig. 9 for the same set of parameters as in Fig. 8. As in the case of $\xi = 0.1$ shown in Fig. 3, the opening angle θ_γ of the emitted photon also concentrates mainly near the value of the opening angle θ_p of the initial vortex electron.

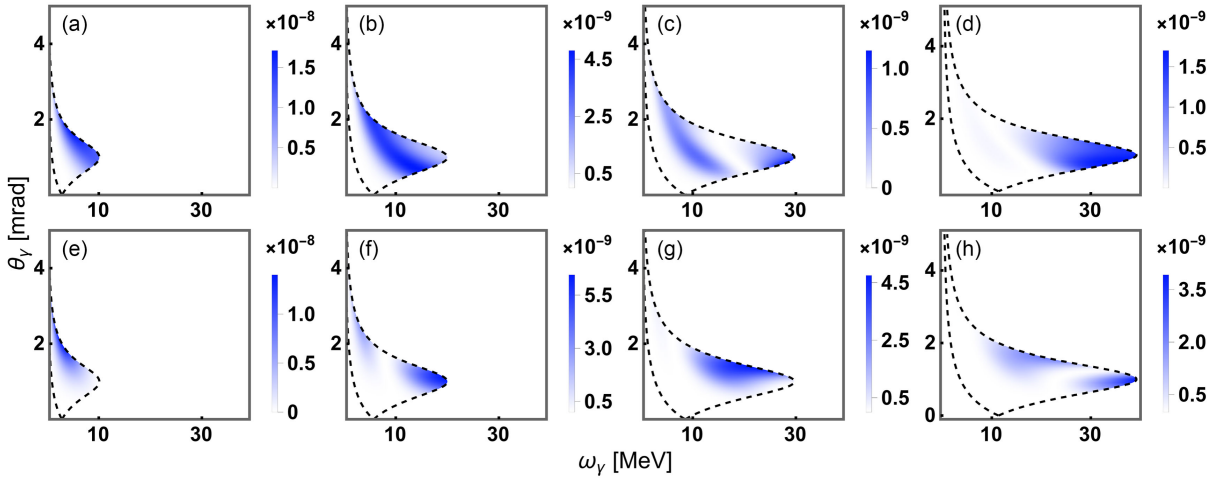


FIG. 9. Same as Fig. 3 except for $\xi = 1$. (a) $\ell_\gamma = 0$, $\lambda = +1$, (b) $\ell_\gamma = 1$, $\lambda = +1$, (c) $\ell_\gamma = 2$, $\lambda = +1$, (d) $\ell_\gamma = 3$, $\lambda = +1$, (e) $\ell_\gamma = 2$, $\lambda = -1$, (f) $\ell_\gamma = 3$, $\lambda = -1$, (g) $\ell_\gamma = 4$, $\lambda = -1$, (h) $\ell_\gamma = 5$, $\lambda = -1$.

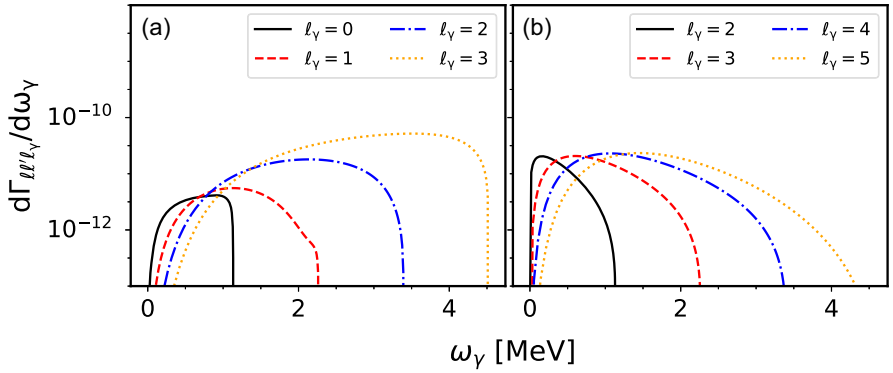


FIG. 10. Same as Fig. 8 except for $\xi = 5$. (a) $\lambda = +1$, (b) $\lambda = -1$.

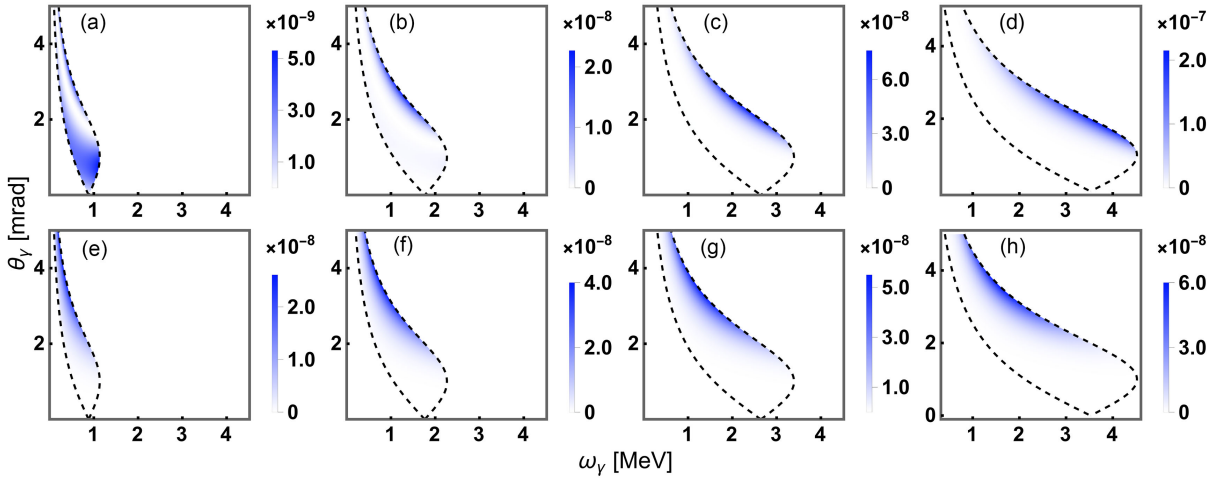


FIG. 11. Same as Fig. 9 except for $\xi = 5$. (a) $\ell_\gamma = 0$, $\lambda = +1$, (b) $\ell_\gamma = 1$, $\lambda = +1$, (c) $\ell_\gamma = 2$, $\lambda = +1$, (d) $\ell_\gamma = 3$, $\lambda = +1$, (e) $\ell_\gamma = 2$, $\lambda = -1$, (f) $\ell_\gamma = 3$, $\lambda = -1$, (g) $\ell_\gamma = 4$, $\lambda = -1$, (h) $\ell_\gamma = 5$, $\lambda = -1$.

TABLE I. The total rate $\Gamma_{\ell\ell'\ell_\gamma}$ in a linearly polarized laser for some value of (ℓ', ℓ_γ). Other parameters are, $\ell = 10$, $\sigma = \sigma' = +1$, $\lambda = +1$, $\theta_p = 1$ mrad, and $\xi = 0.1$.

(ℓ', ℓ_γ)	(10, 0)	(10, 1)	(10, 10)	(10, −10)	(0, 1)	(20, 1)
$\Gamma_{\ell\ell'\ell_\gamma}$ [MeV]	1.7×10^{-13}	1.6×10^{-15}	5.3×10^{-34}	8.6×10^{-31}	4.0×10^{-27}	5.1×10^{-35}

The calculation is also performed for the case $\xi = 5$, with the results presented in Figs. 10 and 11. The rate becomes even larger, and the nonlinear effect becomes strong as demonstrated in the increase of the rate with the photon's ℓ_γ which demands a larger harmonic number n. It is also shown in Figs. 10 and 11 that the maximal energy of the emitted photon in the case $\xi = 5$ is much smaller than the one with a smaller ξ. This is because a larger ξ leads to a heavier dressed mass for the electron, which limits the radiated photon energy as in the plane-wave electron case. Finally, Fig. 11 shows that the opening angle θ_γ of the emitted photon for most values of ℓ_γ is located in the range that is slightly larger than the opening angle θ_p of the initial vortex electron.

C. Linearly polarized laser

Since the photons of a linearly polarized laser are not in a helicity eigenstate, we cannot formulate a constraint on the initial and final particles from angular momentum conservation. In this situation the emitted photon's ℓ_γ does not have a fixed relation with the harmonic number n of the laser. This means that we have to sum over n for a given set of $(\ell, \ell', \ell_\gamma)$. In numerical calculations, we calculate up to a certain value of n in each case where the result has converged safely. In this circumstance we recall from Sec. II C 2 that n has the opposite parity to $\Delta\ell$ for the electron spin-preserved case and the same parity as $\Delta\ell$ for the spin-flipped case. Furthermore, as the Bessel function $J_\nu(\beta)$ in Eq. (56) is extremely suppressed when $\beta \ll \nu$, the summation over ν for the calculation of the amplitude can be safely truncated at a finite ν.

Before presenting distributions we show in Table I the total rate $\Gamma_{\ell\ell'\ell_\gamma}$ for some selected sets of (ℓ', ℓ_γ) with a fixed $\ell = 10$ and $\lambda = +1$. We restrict our discussion to the case when the vortex electron with a small opening angle $\theta_p = 1$ mrad preserves its spin, $\sigma' = \sigma = +1$, and for a not so intense laser $\xi = 0.1$. We observe that $\Gamma_{\ell\ell'\ell_\gamma}$ for small $|\ell - \ell'|$ and $|\ell_\gamma|$ is much larger than the one for a large $|\ell - \ell'|$ or $|\ell_\gamma|$. The suppression in the rate by the increase of $|\ell - \ell'|$ is similar to that in the circularly polarized laser case. The spectrum $d\Gamma_{\ell\ell'\ell_\gamma}/d\omega_\gamma$ of the emitted vortex γ photon is presented in Fig. 12. A multipeak or step-function-like structure is clearly visible. This feature reveals the start-up contribution from each increasing value of n. On inspecting Figs. 12(a) and 12(b), we observe that $d\Gamma_{\ell\ell'\ell_\gamma}/d\omega_\gamma$ with a given ℓ_γ in the case of $\lambda = +1$ looks very similar to the one with a sign-flipped $-\ell_\gamma$ in the case of $\lambda = -1$. As a matter of fact, the corresponding spectra coincide, as can be understood analytically through Eqs. (57a), (57b), and (C5). The nonvanishing of the G functions requires that ℓ_γ has an opposite parity to the harmonic number n when $\ell' = \ell$ as is the case shown in Fig. 12. Furthermore, each G function is a product of two Bessel functions with identical arguments but different orders which interchange when the signs of ℓ_γ and λ are simultaneously flipped. Finally, within the energy range of each step no single ℓ_γ dominates the spectrum. This is a reflection of the fact that there is no manifest angular

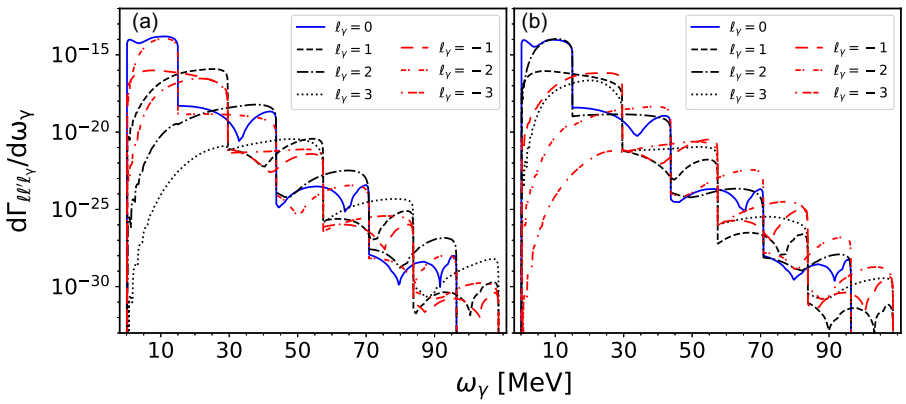


FIG. 12. The distribution $d\Gamma_{\ell\ell'\ell_\gamma}/d\omega_\gamma$ of the emitted vortex γ photon in the linearly polarized laser case and for $\lambda = +1$ ($\lambda = -1$) is shown in panel (a) [panel (b)]. In both panels $\ell = \ell' = 10$, $\sigma = \sigma' = +1$, $\theta_p = 1$ mrad, and $\xi = 0.1$. (a) $\lambda = +1$, (b) $\lambda = -1$.

momentum conservation in a linearly polarized laser, and implies that it would be difficult to isolate a single vortex photon with a given OAM in such a case.

IV. CONCLUSION

We have studied the process of all-vortex nonlinear Compton scattering in an intense and polarized laser field, in which the initial and final electrons and the emitted γ photon are all in vortex states. We have developed a formalism for the process, which allows us to study the exchanges of the OAM and spin angular momentum among the electron, γ photon, and laser. Both circularly and linearly polarized lasers have been investigated.

Our numerical results have shown that, with a less intense laser intensity ($\xi = 0.1$) and a relativistic initial electron, the spectrum $d\Gamma_{\ell\ell'\ell_\gamma}/d\omega_\gamma$ of the emitted vortex γ photon has a strong dependence on the emitted photon's topological charge ℓ_γ and can change by orders of magnitude with different ℓ_γ. Together with the strong ℓ_γ dependence of the range of the energy of the emitted photon, this could offer a possible scenario to separate emitted vortex γ photons with different ℓ_γ. A multipeak structure in the spectrum was found, which depends strongly on the OAMs of the involved particles and the spins of the electrons, as well as the helicity of the γ photon. This could offer a possible way to identify the OAM and spin of the particle. The suppression on the rate and $d\Gamma_{\ell\ell'\ell_\gamma}/d\omega_\gamma$ from the difference between the OAMs of the initial and final vortex electrons has been revealed also. The strong impact of the opening angle of the initial vortex electron has been demonstrated, especially for the electron spin-flipped case. For a high laser intensity ($\xi = 1$ or $\xi = 5$), our numerical calculations have shown that the nonlinear effect is strong. The rate generally increases with the laser intensity. Different from the low-laser-intensity case ($\xi = 0.1$), the order of magnitude of the spectrum stays similar (at $\xi = 1$) or even increases (at $\xi = 5$) when ℓ_γ increases. This implies that a higher laser intensity does not help to isolate an emitted vortex photon with a given definite OAM although it induces a larger average OAM.

ACKNOWLEDGMENTS

This work was supported in part by the Grants No. NSFC-12035008 and No. NSFC-12475122, by the Guangdong Major Project of Basic and Applied Basic Research No. 2020B0301030008, and by the Fundamental Research Funds for the Central Universities (Grant No. 010-63253121).

DATA AVAILABILITY

No data were created or analyzed in this study.

APPENDIX A: CALCULATION OF THE CURRENT FOR A BESSEL-VOLKOV SOLUTION

The Bessel-Volkov solution in Eq. (10a) reads in light-front coordinates

$$\psi^{(a)}_{p_+\kappa\ell\sigma}(x) = N^{\mathrm{B}}_p e^{-i(x_+p_- + x_-p_+)/2} e^{i\phi^p_a} i^{-\ell} \times \sqrt{\frac{\kappa}{2\pi}}\left(1 + \frac{\not{\Omega}\not{a}}{2p\cdot\Omega}\right) W, \tag{A1}$$

where [95]

$$\phi^p_a = \int^\tau d\tau' \frac{a^2(\tau')}{2p\cdot\Omega}, \tag{A2a}$$

$$W = \int \frac{d\phi_p}{2\pi} e^{i\ell\phi_p} e^{i\Xi} u(p,\sigma), \tag{A2b}$$

$$\Xi = \mathbf{p}_\perp \cdot \mathcal{R}_\perp = \kappa\mathcal{R}_\perp \cos(\phi_p - \phi_\mathcal{R}), \tag{A2c}$$

$$\mathcal{R}_\perp = \mathbf{x}_\perp + \frac{1}{p\cdot\Omega}\int^\tau d\tau' \mathbf{a}_\perp(\tau'), \tag{A2d}$$

with $\phi_\mathcal{R}$ being the azimuthal angle of $\mathcal{R}_\perp$. Including the $e^{\pm i\phi_p}$ phases from $u(p,\sigma)$, the ϕ_p integral is finished by shifting $\phi_p \to \phi_p + \phi_\mathcal{R}$ and in terms of the Bessel function,

$$\int_0^{2\pi} \frac{d\phi}{2\pi} e^{i(n\phi + x\cos\phi)} = i^n J_n(x). \tag{A3}$$

The result is [91]

$$W = \begin{pmatrix} \epsilon_+ w_\sigma \\ \epsilon_-\sigma\cos\theta_p w_\sigma \end{pmatrix} e^{i\ell\phi_\mathcal{R}} J_\ell + \begin{pmatrix} 0 \\ w_{-\sigma} \end{pmatrix} i^\sigma e^{i(\ell+\sigma)\phi_\mathcal{R}} J_{\ell+\sigma}\epsilon_- \sin\theta_p, \tag{A4}$$

where all Bessel functions share the argument $\kappa\mathcal{R}_\perp$, $\epsilon_\pm = \sqrt{E \pm M}$, and θ_p is the (half) cone angle of the Bessel vortex. Note that W has a definite value $\ell + \sigma/2$ of the total angular momentum on the z axis. To form the plus component of the current $j_+ = \bar{\psi}^{(a)}_{p_+\kappa\ell\sigma}\gamma_+\psi^{(a)}_{p_+\kappa\ell\sigma}$, we recall that the laser propagates in the $(-z)$ direction $(\Omega_+ = \Omega_\perp = 0)$ so that $\not{\Omega} = \Omega_-\gamma_+/2, \not{\Omega}\gamma_+ = \gamma_+\not{\Omega} = 0$, and thus

$$\begin{aligned} j_+ &= (N^{\mathrm{B}}_p)^2 \frac{\kappa}{2\pi}\bar{W}\gamma_+ W \\ &= (N^{\mathrm{B}}_p)^2 \frac{\kappa}{2\pi}[(\epsilon_+ + \epsilon_-\cos\theta_p)^2 (J_\ell)^2 \\ &\quad + \epsilon_-^2 \sin^2\theta_p (J_{\ell+\sigma})^2]. \end{aligned} \tag{A5}$$

Requiring the normalization condition

$$\frac{1}{2}\int dx_- d^2\mathbf{x}_\perp j_+ = 1, \tag{A6}$$

and noting that $\mathcal{R}_\perp$ differs from $\mathbf{x}_\perp$ by a term that does not depend on $\mathbf{x}_\perp$, the condition becomes

$$1 = \frac{1}{2}(N_p^{\mathrm{B}})^2 \frac{\kappa}{2\pi}\int dx_- 2\pi\mathcal{R}_\perp d\mathcal{R}_\perp [(\epsilon_+ + \epsilon_- \cos\theta_p)^2 (J_\ell)^2 + \epsilon_-^2 \sin^2\theta_p (J_{\ell+\sigma})^2]. \tag{A7}$$

Regularizing the minus coordinate by a large L_- and the radius of the transverse plane by a large R, and using

$$\int_0^R r dr (J_\ell(\kappa r))^2 = \frac{R}{\pi\kappa}, \quad R\to\infty, \tag{A8}$$

we finally obtain

$$N_p^{\mathrm{B}} = \frac{1}{\sqrt{2p_+}}\sqrt{\frac{2\pi}{RL_-}}, \tag{A9}$$

which is the same as that in free space, Eq. (12a).

APPENDIX B: PLANAR INTEGRALS

The δ function in planar polar coordinates can be determined from its Descartes form as follows:

$$\int\int d^2\mathbf{x}\delta^2(\mathbf{x}-\mathbf{x}_0) f(\mathbf{x}) = f(\mathbf{x}_0) \tag{B1a}$$

$$\int\int \rho d\rho d\varphi 2\delta(\rho^2-\rho_0^2)\delta(\varphi-\varphi_0) f(\rho,\varphi) = \int\int d\rho^2 d\varphi \delta(\rho^2-\rho_0^2)\delta(\varphi-\varphi_0) f(\rho,\varphi) = f(\rho_0,\varphi_0) \tag{B1b}$$

$$\Rightarrow \delta^2(\mathbf{x}-\mathbf{x}_0) = 2\delta(\rho^2-\rho_0^2)\delta(\varphi-\varphi_0) = \rho_0^{-1}\delta(\rho-\rho_0)\delta(\varphi-\varphi_0) \quad \text{for } \rho_0 > 0. \tag{B1c}$$

Consider the planar integral [89]

$$J = \int\int d\varphi_1 d\varphi_2 \delta^2(\mathbf{k}_1+\mathbf{k}_2-\mathbf{k}) f(\varphi_1,\varphi_2). \tag{B2}$$

The δ function requires the three vectors to form a triangle. Given their magnitudes, there are two solutions as can be seen geometrically: drawing one circle of radius $|\mathbf{k}_1| = k_1$ at one end of $\mathbf{k}$ and another circle of radius $|\mathbf{k}_2| = k_2$ at the other end, the two circles intersect at two points which are the solutions,

$$\angle(\mathbf{k},\mathbf{k}_{1,2}) = \delta_{1,2} = \arccos\frac{k^2+k_{1,2}^2-k_{2,1}^2}{2kk_{1,2}}, \tag{B3a}$$

$$2\mathbf{k}\cdot\mathbf{k}_{1,2} = k^2+k_{1,2}^2-k_{2,1}^2, \tag{B3b}$$

$$\varphi_k-\varphi_1 = \pm\delta_1, \qquad \varphi_k-\varphi_2 = \mp\delta_2. \tag{B3c}$$

Then, we have

$$J = \int\int d\varphi_1 d\varphi_2 2\delta(\mathbf{k}_1^2-(\mathbf{k}-\mathbf{k}_2)^2)\delta(\varphi_1-\varphi_{\mathbf{k}-\mathbf{k}_2}) f(\varphi_1,\varphi_2) = 2\int d\varphi_2 \delta(k_1^2-k^2-k_2^2+2kk_2\cos(\varphi_2-\varphi_k)) f(\varphi_{\mathbf{k}-\mathbf{k}_2},\varphi_2) = \frac{1}{2\Delta}[f(\varphi_k-\delta_1,\varphi_k+\delta_2)+f(\varphi_k+\delta_1,\varphi_k-\delta_2)], \tag{B4}$$

where Δ is the area of the triangle:

$$\Delta = \frac{1}{2}kk_2\sin\delta_2 = \frac{1}{4}\sqrt{-\lambda(k_1^2,k_2^2,k^2)}. \tag{B5}$$

APPENDIX C: BASIC ANGULAR INTEGRAL IN A LINEARLY POLARIZED LASER

The basic azimuthal integral to be evaluated in a linearly polarized case is,

$$G_\mu^m(\eta) = \int_0^{2\pi} d\varphi e^{im\varphi} J_\mu(\gamma^{\mathrm{L}}), \tag{C1}$$

where $\gamma^{\mathrm{L}} = \sqrt{2}\gamma^{\mathrm{C}}\cos(\varphi-\eta\varphi_0)$, m, μ are both integers, $\eta = \pm 1$, and only the parameters relevant to the calculation of the integral are indicated in G. Shifting $\varphi\to\varphi+\eta\varphi_0$ gives

$$G_\mu^m(\eta) = e^{im\eta\varphi_0} H_\mu^m, \tag{C2a}$$

$$H_\mu^m = \int_b^{b+2\pi} d\varphi\, e^{im\varphi} J_\mu(2a\,\cos\varphi), \tag{C2b}$$

where $a = \gamma^{\mathrm{C}}/\sqrt{2}$ and $b = -\eta\varphi_0$. The integrand of H_μ^m is a periodic function of φ in the interval and thus H_μ^m actually does not depend on the choice of b. To apply formulas (6.681)-8 and -9 in Ref. [99], we first focus on the case with integers $\mu \geq 0$ and m arbitrary, and will come back to the case of $\mu < 0$ by using $J_{-\mu}(z) = (-1)^\mu J_\mu(z)$. Choosing $b = \pi/2$, shifting $\varphi\to\varphi+\pi/2$, and then using $J_\mu(-z) = (-1)^\mu J_\mu(z)$, we have

$$H_\mu^m = i^m(-1)^\mu \int_0^{2\pi} d\varphi\, e^{im\varphi} J_\mu(2a\,\sin\varphi). \tag{C3}$$

We cut the interval into two halves, and for the upper half we shift $\varphi\to\varphi+\pi$, so that

$$H_\mu^m = i^m[(-1)^\mu+(-1)^m]\int_0^\pi d\varphi\, e^{im\varphi} J_\mu(2a\,\sin\varphi) = i^m[(-1)^\mu+(-1)^m] i^m \pi J_{(\mu+m)/2}(a) J_{(\mu-m)/2}(a) = [1+(-1)^{\mu+m}]\pi J_{(\mu+m)/2}(a) J_{(\mu-m)/2}(a). \tag{C4}$$

In summary, for $\mu \geq 0$,

$$G_\mu^m(\eta) = [1+(-1)^{\mu+m}]e^{im\eta\varphi_0}\pi J_{(\mu+m)/2}(\gamma^C/\sqrt{2}) \times J_{(\mu-m)/2}(\gamma^C/\sqrt{2}), \tag{C5}$$

which requires integers μ, m to have the same parity to be nonvanishing. For $\mu < 0$, we use $J_{-\mu}(z) = (-1)^\mu J_\mu(z)$ to obtain

$$\begin{aligned} G_\mu^m(\eta) &= e^{im\eta\varphi_0}(-1)^\mu \int_0^{2\pi} d\varphi\, e^{im\varphi} J_{-\mu}(\sqrt{2}\gamma^C\cos\varphi) \\ &= e^{im\eta\varphi_0}(-1)^\mu[1+(-1)^{-\mu+m}]\pi J_{(-\mu+m)/2}(\gamma^C/\sqrt{2}) \\ &\quad \times J_{(-\mu-m)/2}(\gamma^C/\sqrt{2}) \\ &= e^{im\eta\varphi_0}[1+(-1)^{\mu+m}]\pi J_{(\mu+m)/2}(\gamma^C/\sqrt{2}) \\ &\quad \times J_{(\mu-m)/2}(\gamma^C/\sqrt{2}), \end{aligned} \tag{C6}$$

i.e., the result generally applies for any integers μ and m.

APPENDIX D: INTEGRAL OVER κ

We transform in Sec. II D 2 the original integral over κ to the following form:

$$I = \int_{x_1}^{x_2} dx \frac{g(x)}{\sqrt{(x_2-x)(x-x_1)}}, \tag{D1}$$

where $g(x)$ is a smooth function. To isolate the apparent singularities at the end points, we make subtractions:

$$\begin{aligned} I = &\int_{x_1}^{x_2} dx \left(\frac{1}{\sqrt{x_2-x}} - \frac{1}{\sqrt{x_2-x_1}}\right) \\ &\times \left(\frac{1}{\sqrt{x-x_1}} - \frac{1}{\sqrt{x_2-x_1}}\right) g(x) \\ &+ \frac{1}{\sqrt{x_2-x_1}} \int_{x_1}^{x_2} dx \left(\frac{1}{\sqrt{x-x_1}} + \frac{1}{\sqrt{x_2-x}}\right) g(x) \\ &- \frac{1}{x_2-x_1} \int_{x_1}^{x_2} dx g(x). \end{aligned} \tag{D2}$$

The integrand in the first integral vanishes at the end points and is thus well behaved. Each integrand in the second integral is singular only at one end point and is easy to cope with. It can be further softened by using integration by parts:

$$\int_{x_1}^{x_2} dx \frac{g(x)}{\sqrt{x-x_1}} = 2g(x_2)\sqrt{x_2-x_1} - 2\int dx g'(x)\sqrt{x-x_1}, \tag{D3a}$$

$$\int_{x_1}^{x_2} dx \frac{g(x)}{\sqrt{x_2-x}} = 2g(x_1)\sqrt{x_2-x_1} + 2\int dx g'(x)\sqrt{x_2-x}. \tag{D3b}$$

To make the first integral numerically amenable, we combine the square roots:

$$\begin{aligned} &\left(\frac{1}{\sqrt{x_2-x}} - \frac{1}{\sqrt{x_2-x_1}}\right)\left(\frac{1}{\sqrt{x-x_1}} - \frac{1}{\sqrt{x_2-x_1}}\right) \\ &= \frac{1}{x_2-x_1} \frac{\sqrt{(x_2-x)(x-x_1)}}{(\sqrt{x_2-x_1}+\sqrt{x_2-x})(\sqrt{x_2-x_1}+\sqrt{x-x_1})}. \end{aligned} \tag{D4}$$

In summary, the final form is,

$$\begin{aligned} I = &-\frac{1}{x_2-x_1} \\ &\times \int_{x_1}^{x_2} dx \frac{(x_2-x_1)+\sqrt{x_2-x_1}(\sqrt{x-x_1}+\sqrt{x_2-x})}{(\sqrt{x_2-x_1}+\sqrt{x_2-x})(\sqrt{x_2-x_1}+\sqrt{x-x_1})} g(x) \\ &+ \frac{2}{\sqrt{x_2-x_1}} \int dx g'(x)(\sqrt{x_2-x}-\sqrt{x-x_1}) \\ &+ 2[g(x_1)+g(x_2)]. \end{aligned} \tag{D5}$$

[1] K. Y. Bliokh and F. Nori, Transverse and longitudinal angular momenta of light, Phys. Rep. **592**, 1 (2015).

[2] B. A. Knyazev and V. G. Serbo, Beams of photons with nonzero projections of orbital angular momenta: New results, Phys. Usp. **61**, 449 (2018).

[3] K. Y. Bliokh *et al.*, Theory and applications of free-electron vortex states, Phys. Rep. **690**, 1 (2017).

[4] S. M. Lloyd, M. Babiker, G. Thirunavukkarasu, and J. Yuan, Electron vortices: Beams with orbital angular momentum, Rev. Mod. Phys. **89**, 035004 (2017).

[5] I. P. Ivanov, Promises and challenges of high-energy vortex states collisions, Prog. Part. Nucl. Phys. **127**, 103987 (2022).

[6] A. M. Yao and M. J. Padgett, Orbital angular momentum: Origins, behavior and applications, Adv. Opt. Photonics **3**, 161 (2011).

[7] Y. Shen, X. Wang, Z. Xie, C. Min, X. Fu, Q. Liu, M. Gong, and X. Yuan, Optical vortices 30 years on: OAM manipulation from topological charge to multiple singularities, Light Sci. Appl. **8**, 90 (2019).

[8] A. Forbes, L. Mkhumbuza, and L. Feng, Orbital angular momentum lasers, Nat. Rev. Phys. **6**, 352 (2024).
[9] L. Allen, M. W. Beijersbergen, R. J. C. Spreeuw, and J. P. Woerdman, Orbital angular momentum of light and the transformation of Laguerre-Gaussian laser modes, Phys. Rev. A **45**, 8185 (1992).
[10] M. Beijersbergen, R. Coerwinkel, M. Kristensen, and J. Woerdman, Helical-wavefront laser beams produced with a spiral phaseplate, Opt. Commun. **112**, 321 (1994).
[11] S. S. R. Oemrawsingh, J. A. W. van Houwelingen, E. R. Eliel, J. P. Woerdman, E. J. K. Verstegen, J. G. Kloosterboer, and G. W. 't Hooft, Production and characterization of spiral phase plates for optical wavelengths, Appl. Opt. **43**, 688 (2004).
[12] G. Ruffato, M. Massari, and F. Romanato, Generation of high-order Laguerre Gaussian modes by means of spiral phase plates, Opt. Lett. **39**, 5094 (2014).
[13] A. Longman, C. Salgado, G. Zeraouli, J. I. A. naniz, J. A. Pérez-Hernández, M. K. Eltahlawy, L. Volpe, and R. Fedosejevs, Off-axis spiral phase mirrors for generating high-intensity optical vortices, Opt. Lett. **45**, 2187 (2020).
[14] N. R. Heckenberg, R. McDuff, C. P. Smith, and A. G. White, Generation of optical phase singularities by computer-generated holograms, Opt. Lett. **17**, 221 (1992).
[15] A. G. Peele, P. J. McMahon, D. Paterson, C. Q. Tran, A. P. Mancuso, K. A. Nugent, J. P. Hayes, E. Harvey, B. Lai, and I. McNulty, Observation of an x-ray vortex, Opt. Lett. **27**, 1752 (2002).
[16] B. Terhalle, A. Langner, B. Päivänranta, V. A. Guzenko, C. David, and Y. Ekinci, Generation of extreme ultraviolet vortex beams using computer generated holograms, Opt. Lett. **36**, 4143 (2011).
[17] G. Gariepy, J. Leach, K. T. Kim, T. J. Hammond, E. Frumker, R. W. Boyd, and P. B. Corkum, Creating high-harmonic beams with controlled orbital angular momentum, Phys. Rev. Lett. **113**, 153901 (2014).
[18] E. Hemsing, A. Knyazik, M. Dunning, D. Xiang, A. Marinelli, C. Hast, and J. B. Rosenzweig, Coherent optical vortices from relativistic electron beams, Nat. Phys. **9**, 549 (2013).
[19] J. Bahrdt, K. Holldack, P. Kuske, R. Müller, M. Scheer, and P. Schmid, First observation of photons carrying orbital angular momentum in undulator radiation, Phys. Rev. Lett. **111**, 034801 (2013).
[20] D. C. Gauthier *et al.*, Tunable orbital angular momentum in high-harmonic generation, Nat. Commun. **8**, 14971 (2016).
[21] J. C. T. Lee, S. J. Alexander, S. D. Kevan, S. Roy, and B. J. McMorran, Laguerre–Gauss and Hermite–Gauss soft x-ray states generated using diffractive optics, Nat. Photonics **13**, 205 (2019).
[22] M. Uchida and A. Tonomura, Generation of electron beams carrying orbital angular momentum, Nature (London) **464**, 737 (2010).
[23] J. Verbeeck, H. Tian, and P. Schattschneider, Production and application of electron vortex beams, Nature (London) **467**, 301 (2010).
[24] B. J. McMorran, A. Agrawal, I. M. Anderson, A. A. Herzing, H. J. Lezec, J. J. McClelland, and J. Unguris, Electron vortex beams with high quanta of orbital angular momentum, Science **331**, 1198804 (2011).
[25] E. Mafakheri, A. H. Tavabi, P.-H. Lu, R. Balboni, F. Venturi, C. Menozzi, G. C. Gazzadi, S. Frabboni, A. Sit, R. E. Dunin-Borkowski, E. Karimi, and V. Grillo, Realization of electron vortices with large orbital angular momentum using miniature holograms fabricated by electron beam lithography, Appl. Phys. Lett. **110**, 093113 (2017).
[26] A. H. Tavabi, P. Rosi, A. Roncaglia, E. Rotunno, M. Beleggia, P.-H. Lu, L. Belsito, G. Pozzi, S. Frabboni, P. Tiemeijer, R. E. Dunin-Borkowski, and V. Grillo, Generation of electron vortex beams with over 1000 orbital angular momentum quanta using a tunable electrostatic spiral phase plate, Appl. Phys. Lett. **121**, 073506 (2022).
[27] G. M. Vanacore, G. Berruto, I. Madan, E. Pomarico, P. Biagioni, R. Lamb, D. McGrouther, O. Reinhardt, I. Kaminer, B. Barwick *et al.*, Ultrafast generation and control of an electron vortex beam via chiral plasmonic near fields, Nat. Mater. **18**, 573 (2019).
[28] C. W. Clark, R. Barankov, M. G. Huber, M. Arif, D. G. Cory, and D. A. Pushin, Controlling neutron orbital angular momentum, Nature (London) **525**, 504 (2015).
[29] D. Sarenac, C. Kapahi, W. Chen, C. W. Clark, D. G. Cory, M. G. Huber, I. Taminiau, K. Zhernenkov, and D. A. Pushin, Generation and detection of spin-orbit coupled neutron beams, Proc. Natl. Acad. Sci. U.S.A. **116**, 20328 (2019).
[30] D. Sarenac, M. E. Henderson, H. Ekinci, C. W. Clark, D. G. Cory, L. DeBeer-Schmitt, M. G. Huber, C. Kapahi, and D. A. Pushin, Experimental realization of neutron helical waves, Sci. Adv. **8**, eadd2002 (2022).
[31] A. Luski, Y. Segev, R. David, O. Bitton, H. Nadler, A. R. Barnea, A. Gorlach, O. Cheshnovsky, I. Kaminer, and E. Narevicius, Vortex beams of atoms and molecules, Science **373**, 1105 (2021).
[32] A. Mair, A. Vaziri, G. Weihs, and A. Zeilinger, Entanglement of the orbital angular momentum states of photons, Nature (London) **412**, 313 (2001).
[33] X.-L. Wang, X.-D. Cai, Z.-E. Su, M.-C. Chen, D. Wu, L. Li, N.-L. Liu, C.-Y. Lu, and J.-W. Pan, Quantum teleportation of multiple degrees of freedom of a single photon, Nature (London) **518**, 516 (2015).
[34] H. He, M. E. J. Friese, N. R. Heckenberg, and H. Rubinsztein-Dunlop, Direct observation of transfer of angular momentum to absorptive particles from a laser beam with a phase singularity, Phys. Rev. Lett. **75**, 826 (1995).
[35] N. B. Simpson, K. Dholakia, L. Allen, and M. J. Padgett, Mechanical equivalence of spin and orbital angular momentum of light: An optical spanner, Opt. Lett. **22**, 52 (1997).
[36] D. G. Grier, A revolution in optical manipulation, Nature (London) **424**, 810 (2003).
[37] H. Larocque, I. Kaminer, V. Grillo, R. W. Boyd, and E. Karimi, Twisting neutrons may reveal their internal structure, Nat. Phys. **14**, 1 (2018).
[38] I. Kaminer, J. Nemirovsky, M. Rechtsman, R. Bekenstein, and M. Segev, Self-accelerating Dirac particles and

prolonging the lifetime of relativistic fermions, Nat. Phys. **11**, 261 (2015).
[39] I. Madan, G. M. Vanacore, S. Gargiulo, T. LaGrange, and F. Carbone, The quantum future of microscopy: Wave function engineering of electrons, ions, and nuclei, Appl. Phys. Lett. **116**, 230502 (2020).
[40] A. Picón, A. Benseny, J. Mompart, J. R. Vázquez de Aldana, L. Plaja, G. F. Calvo, and L. Roso, Transferring orbital and spin angular momenta of light to atoms, New J. Phys. **12**, 083053 (2010).
[41] A. Afanasev, C. E. Carlson, and A. Mukherjee, High-multipole excitations of hydrogen-like atoms by twisted photons near a phase singularity, J. Opt. **18**, 074013 (2016).
[42] V. Serbo, I. P. Ivanov, S. Fritzsche, D. Seipt, and A. Surzhykov, Scattering of twisted relativistic electrons by atoms, Phys. Rev. A **92**, 012705 (2015).
[43] D. V. Karlovets, G. L. Kotkin, V. G. Serbo, and A. Surzhykov, Scattering of twisted electron wave packets by atoms in the Born approximation, Phys. Rev. A **95**, 032703 (2017).
[44] D. V. Karlovets, G. L. Kotkin, and V. G. Serbo, Scattering of wave packets on atoms in the Born approximation, Phys. Rev. A **92**, 052703 (2015).
[45] A. V. Maiorova, S. Fritzsche, R. A. Mueller, and A. Surzhykov, Elastic scattering of twisted electrons by diatomic molecules, Phys. Rev. A **98**, 042701 (2018).
[46] A. Mandal, N. Dhankhar, D. Sébilleau, and R. Choubisa, Semirelativistic $(e, 2e)$ study with a twisted electron beam on Cu and Ag, Phys. Rev. A **104**, 052818 (2021).
[47] M. E. Groshev, V. A. Zaytsev, V. A. Yerokhin, and V. M. Shabaev, Bremsstrahlung from twisted electrons in the field of heavy nuclei, Phys. Rev. A **101**, 012708 (2020).
[48] A. J. Silenko, P. Zhang, and L. Zou, Electric quadrupole moment and the tensor magnetic polarizability of twisted electrons and a potential for their measurements, Phys. Rev. Lett. **122**, 063201 (2019).
[49] A. G. Hayrapetyan, O. Matula, A. Aiello, A. Surzhykov, and S. Fritzsche, Interaction of relativistic electron-vortex beams with few-cycle laser pulses, Phys. Rev. Lett. **112**, 134801 (2014).
[50] P. Bandyopadhyay, B. Basu, and D. Chowdhury, Relativistic electron vortex beams in a laser field, Phys. Rev. Lett. **115**, 194801 (2015).
[51] I. A. Aleksandrov, D. A. Tumakov, A. Kudlis, V. A. Zaytsev, and N. N. Rosanov, Scattering of a twisted electron wavepacket by a finite laser pulse, Phys. Rev. A **106**, 033119 (2022).
[52] Y. Wu, S. Gargiulo, F. Carbone, C. H. Keitel, and A. Pálffy, Dynamical control of nuclear isomer depletion via electron vortex beams, Phys. Rev. Lett. **128**, 162501 (2022).
[53] Z.-W. Lu *et al.*, Manipulation of giant multipole resonances via vortex γ photons, Phys. Rev. Lett. **131**, 202502 (2023).
[54] D. Sarenac *et al.*, Small-angle scattering interferometry with neutron orbital angular momentum states, Nat. Commun. **15**, 10785 (2024).
[55] Z.-W. Lu, L. Guo, M. Ababekri, J.-l. Zhang, X.-F. Weng, Y. Wu, Y.-F. Niu, and J.-X. Li, Angular momentum resolved inelastic electron scattering for nuclear giant resonances, Phys. Rev. Lett. **134**, 052501 (2025).
[56] I. P. Ivanov, N. Korchagin, A. Pimikov, and P. Zhang, Doing spin physics with unpolarized particles, Phys. Rev. Lett. **124**, 192001 (2020).
[57] Y. Xu, D. L. Balabanski, V. Baran, C. Iorga, and C. Matei, Vortex photon induced nuclear reaction: Mechanism, model, and application to the studies of giant resonance and astrophysical reaction rate, Phys. Lett. B **852**, 138622 (2024).
[58] A. Afanasev and C. E. Carlson, Delta baryon photoproduction with twisted photons, Ann. Phys. (Berlin) **534**, 2100228 (2022).
[59] Z. Bu, L. Ji, S. Lei, H. Hu, X. Zhang, and B. Shen, Twisted Breit-Wheeler electron-positron pair creation via vortex gamma photons, Phys. Rev. Res. **3**, 043159 (2021).
[60] S. Lei, Z. Bu, W. Wang, B. Shen, and L. Ji, Generation of relativistic positrons carrying intrinsic orbital angular momentum, Phys. Rev. D **104**, 076025 (2021).
[61] J. A. Sherwin, Theoretical study of the double Compton effect with twisted photons, Phys. Rev. A **95**, 052101 (2017).
[62] T. Maruyama, T. Hayakawa, and T. Kajino, Compton scattering of γ-ray vortex with Laguerre Gaussian wave function, Sci. Rep. **9**, 51 (2019).
[63] K. Y. Bliokh, M. R. Dennis, and F. Nori, Position, spin, and orbital angular momentum of a relativistic electron, Phys. Rev. A **96**, 023622 (2017).
[64] A. J. Silenko, P. Zhang, and L. Zou, Relativistic quantum-mechanical description of twisted paraxial electron and photon beams, Phys. Rev. A **100**, 030101 (2019).
[65] A. J. Silenko, P. Zhang, and L. Zou, Relativistic quantum dynamics of twisted electron beams in arbitrary electric and magnetic fields, Phys. Rev. Lett. **121**, 043202 (2018).
[66] K. van Kruining, A. G. Hayrapetyan, and J. B. Götte, Nonuniform currents and spins of relativistic electron vortices in a magnetic field, Phys. Rev. Lett. **119**, 030401 (2017).
[67] S. M. Barnett, Relativistic electron vortices, Phys. Rev. Lett. **118**, 114802 (2017).
[68] I. Bialynicki-Birula and Z. Bialynicka-Birula, Relativistic electron wave packets carrying angular momentum, Phys. Rev. Lett. **118**, 114801 (2017).
[69] Z. Bu, L. Ji, X. Geng, S. Liu, S. Lei, B. Shen, R. Li, and Z. Xu, Generation of quantum vortex electrons with intense laser pulses, Adv. Sci. **11**, 2404564 (2024).
[70] Z. Li, S. Liu, B. Liu, L. Ji, and I. P. Ivanov, Unambiguous detection of high-energy vortex states via the superkick effect, Phys. Rev. Lett. **133**, 265001 (2024).
[71] M. Katoh *et al.*, Helical phase structure of radiation from an electron in circular motion, Sci. Rep. **7**, 6130 (2017).
[72] V. Petrillo, G. Dattoli, I. Drebot, and F. Nguyen, Compton scattered x-gamma rays with orbital momentum, Phys. Rev. Lett. **117**, 123903 (2016).
[73] U. D. Jentschura and V. G. Serbo, Generation of high-energy photons with large orbital angular momentum by Compton backscattering, Phys. Rev. Lett. **106**, 013001 (2011).
[74] U. D. Jentschura and V. G. Serbo, Compton upconversion of twisted photons: Backscattering of particles with non-planar wave functions, Eur. Phys. J. C **71**, 1571 (2011).

[75] M. Katoh, M. Fujimoto, H. Kawaguchi, K. Tsuchiya, K. Ohmi, T. Kaneyasu, Y. Taira, M. Hosaka, A. Mochihashi, and Y. Takashima, Angular momentum of twisted radiation from an electron in spiral motion, Phys. Rev. Lett. **118**, 094801 (2017).

[76] Y. Taira, T. Hayakawa, and M. Katoh, Gamma-ray vortices from nonlinear inverse Thomson scattering of circularly polarized light, Sci. Rep. **7**, 5018 (2017).

[77] Y.-Y. Chen, J.-X. Li, K. Z. Hatsagortsyan, and C. H. Keitel, γ -ray beams with large orbital angular momentum via nonlinear Compton scattering with radiation reaction, Phys. Rev. Lett. **121**, 074801 (2018).

[78] M. Ababekri, R.-T. Guo, F. Wan, B. Qiao, Z. Li, C. Lv, B. Zhang, W. Zhou, Y. Gu, and J.-X. Li, Vortex γ photon generation via spin-to-orbital angular momentum transfer in nonlinear Compton scattering, Phys. Rev. D **109**, 016005 (2024).

[79] R.-T. Guo, M. Ababekri, Q. Zhao, Y. I. Salamin, L.-L. Ji, Z.-G. Bu, Z.-F. Xu, X.-F. Weng, and J.-X. Li, Generation of γ photons with extremely large orbital angular momenta, Phys. Rev. A **110**, 032202 (2024).

[80] O. V. Bogdanov, P. O. Kazinski, and G. Y. Lazarenko, Semiclassical probability of radiation of twisted photons in the ultrarelativistic limit, Phys. Rev. D **99**, 116016 (2019).

[81] J.-J. Jiang, K.-H. Zhuang, J.-D. Chen, J.-X. Li, and Y.-Y. Chen, Controlling the polarization and vortex charge of γ photons via nonlinear Compton scattering, Phys. Rev. Lett. **134**, 153802 (2025).

[82] J. Wang, X. Li, L. Gan, Y. Xie, C. Zhong, C. Zhou, S. Zhu, X. He, and B. Qiao, Generation of intense vortex gamma rays via spin-to-orbital conversion of angular momentum in relativistic laser-plasma interactions, Phys. Rev. Appl. **14**, 014094 (2020).

[83] C. Liu, B. Shen, X. Zhang, Y. Shi, L. Ji, W. Wang, L. Yi, L. Zhang, T. Xu, Z. Pei *et al.*, Generation of gamma-ray beam with orbital angular momentum in the QED regime, Phys. Plasmas **23**, 093120 (2016).

[84] Y.-T. Hu, J. Zhao, H. Zhang, Y. Lu, W.-Q. Wang, L.-X. Hu, F.-Q. Shao, and T.-P. Yu, Attosecond γ-ray vortex generation in near-critical-density plasma driven by twisted laser pulses, Appl. Phys. Lett. **118**, 054101 (2021).

[85] L. Ju, C. Zhou, K. Jiang, T. Huang, H. Zhang, T. Cai, J. Cao, B. Qiao, and S. Ruan, Manipulating the topological structure of ultrarelativistic electron beams using Laguerre–Gaussian laser pulse, New J. Phys. **20**, 063004 (2018).

[86] D. Karlovets, Vortex particles in axially symmetric fields and applications of the quantum Busch theorem, New J. Phys. **23**, 033048 (2021).

[87] D. V. Karlovets, S. S. Baturin, G. Geloni, G. K. Sizykh, and V. G. Serbo, Generation of vortex particles via generalized measurements, Eur. Phys. J. C **82**, 1008 (2022).

[88] D. V. Karlovets, S. S. Baturin, G. Geloni, G. K. Sizykh, and V. G. Serbo, Shifting physics of vortex particles to higher energies via quantum entanglement, Eur. Phys. J. C **83**, 372 (2023).

[89] I. P. Ivanov, Colliding particles carrying non-zero orbital angular momentum, Phys. Rev. D **83**, 093001 (2011).

[90] V. B. Berestetskii, E. M. Lifshitz, and L. P. Pitaevskii, *Quantum Electrodynamics (Second Edition)* (Butterworth-Heinemann, Oxford, 1982).

[91] K. Y. Bliokh, M. R. Dennis, and F. Nori, Relativistic electron vortex beams: Angular momentum and spin-orbit interaction, Phys. Rev. Lett. **107**, 174802 (2011).

[92] S. J. Brodsky, H.-C. Pauli, and S. S. Pinsky, Quantum chromodynamics and other field theories on the light cone, Phys. Rep. **301**, 299 (1998).

[93] D. Seipt and B. King, Spin- and polarization-dependent locally-constant-field-approximation rates for nonlinear Compton and Breit-Wheeler processes, Phys. Rev. A **102**, 052805 (2020).

[94] B. King and S. Tang, Nonlinear Compton scattering of polarized photons in plane-wave backgrounds, Phys. Rev. A **102**, 022809 (2020).

[95] D. V. Karlovets, Electron with orbital angular momentum in a strong laser wave, Phys. Rev. A **86**, 062102 (2012).

[96] I. P. Ivanov, Non-forward scattering of twisted particles, arXiv:1101.1630.

[97] I. P. Ivanov and V. G. Serbo, Scattering of twisted particles: Extension to wave packets and orbital helicity, Phys. Rev. A **84**, 033804 (2011).

[98] J. Ponce de Leon, Revisiting the orthogonality of Bessel functions of the first kind on an infinite interval, Eur. J. Phys. **36**, 015016 (2015).

[99] I. Gradshteyn and I. Ryzhik, *Table of Integrals, Series, and Products* (Academic Press, New York, 2007).

[100] G. L. Kotkin, V. G. Serbo, and A. Schiller, Processes with large impact parameters at colliding beams, Int. J. Mod. Phys. A **07**, 4707 (1992).

[101] D. V. Karlovets, V. G. Serbo, and A. Surzhykov, Wave function of a photon produced in the resonant scattering of twisted light by relativistic ions, Phys. Rev. A **104**, 023101 (2021).

[102] A. Gonoskov, T. G. Blackburn, M. Marklund, and S. S. Bulanov, Charged particle motion and radiation in strong electromagnetic fields, Rev. Mod. Phys. **94**, 045001 (2022).